ANALYTICITY OF THE DIRICHLET-NEUMANN OPERATOR AND ITS APPLICATION TO DETECTING OCEAN BATHYMETRY

BY

MARK TABER
B.S. (Pacific Union College) 2002
M.S. (University of Notre Dame) 2004

THESIS

Submitted in partial fulfillment of the requirements
for the degree of Doctor of Philosophy in Mathematics
in the Graduate College of the
University of Illinois at Chicago, 2007

Chicago, Illinois

To my wife,

Brianne.

ACKNOWLEDGMENTS

I would like to thank my parents, whose support and encouragement was much appreciated. I would also like to thank Brent Haloviak and Doug Havens, who were both very instrumental in encouraging and nurturing my early mathematical and scientific education. A debt is also owed to the professors in the mathematics department at Pacific Union College. For a small department at a small school, they prepared me well to meet the challenge of graduate school. Lastly, I would also like to thank my advisor, Dave Nicholls, whose patience I am sure I tested, but it never failed. The encouragement and guidance are much appreciated.

TABLE OF CONTENTS

CHAPTER			PAGE
1	**INTRODUCTION**		1
2	**THE EQUATIONS OF MOTION**		6
	2.1	Navier-Stokes Equations	6
	2.2	Zakharov's Hamiltonian Formulation	8
	2.3	Surface Reformulation	9
3	**THE DIRICHLET-NEUMANN OPERATOR**		11
	3.1	Expansion	11
	3.2	Field Expansion and Operator Expansion	13
	3.3	The Transformed Field Expansion	19
	3.4	Analyticity of the DNO	26
	3.5	Proof of Analyticity	37
4	**A NON-TRADITIONAL INVERSE METHOD FOR DETERMINING BOTTOM TOPOGRAPHY**		42
	4.1	A General Method	42
	4.2	A Partial Expansion of the DNO–Operator Expansion	46
	4.3	Craig's First Order Formula	51
	4.4	A Few Second Order Algorithms	53
	4.4.1	Picard Iteration	54
	4.4.2	Second Order Methods Derived From Factoring	55
	4.5	Higher Order Methods	56
	4.5.1	M^{th} Order Picard	58
	4.5.2	M^{th} Order Left Factorization	58
5	**NUMERICAL RESULTS**		60
	5.1	Method for Numerical Testing	60
	5.2	Convergence	62
	5.3	Representative Results	62
	5.4	Variation of Parameters in $\zeta_1(x)$	66
	5.5	Variation of Parameters in $\zeta_2(x)$	69
	5.6	Noise	75
	5.7	Representative Results–Miscellaneous Bottom Contours	75
6	**CONCLUSIONS**		80
	6.1	The Expansion of the DNO	80

TABLE OF CONTENTS (Continued)

CHAPTER		PAGE
6.2	Comparison of Various Methods	80
6.3	Future Directions	81
APPENDICES		82
Appendix A		83
CITED LITERATURE		86
VITA		89

LIST OF FIGURES

FIGURE		PAGE
1a	Convergence of Methods for $\zeta^{(1)}$	63
1b	Convergence of Methods for $\zeta^{(2)}$	63
2a	Convergence Towards Input for $\zeta^{(1)}$	64
2b	Convergence Towards Input for $\zeta^{(2)}$	64
3a	Error vs. Number of Gridpoints for $\zeta^{(1)}$	65
3b	Error vs. Number of Gridpoints for $\zeta^{(2)}$	65
4a	Representative Results For $\zeta^{(1)}$	67
4b	Representative Results For $\zeta^{(2)}$	67
5a	Magnified Representative Results For $\zeta^{(1)}$	68
5b	Magnified Representative Results For $\zeta^{(2)}$	68
6a	Error vs. a for $\zeta^{(1)}$	70
6b	Error vs. b for $\zeta^{(1)}$	70
6c	Error vs. h for $\zeta^{(1)}$	71
7a	Error vs. a for $\zeta^{(2)}$	73
7b	Error vs. b for $\zeta^{(2)}$	73
7c	Error vs. c for $\zeta^{(2)}$	74
7d	Error vs. h for $\zeta^{(2)}$	74
8a	Error vs. Noise Magnitude in $\overline{\eta}$ for $\zeta^{(1)}$	76
8b	Error vs. Noise Magnitude in $\overline{\eta}$ for $\zeta^{(2)}$	76

LIST OF FIGURES (Continued)

FIGURE		PAGE
9a	Error vs. Noise Magnitude in ω for $\zeta^{(1)}$	77
9b	Error vs. Noise Magnitude in ω for $\zeta^{(2)}$	77
10a	Limiting Case When $c \to \infty$	78
10b	Representative Results When ζ Has a Sharp Corner	78
10c	Representative Results When ζ is Not Symmetrical	79

LIST OF ABBREVIATIONS

DNO	Dirichlet-Neumann Operator
FE	Field Expansion
OE	Operator Expansion
TFE	Transformed Field Expansion
2P	Second-Order Picard Method
2L	Second-Order Left-Factored Method
2R	Second-Order Right-Factored Method
5P	Fifth-Order Picard Method
5L	Fifth-Order Left-Factored Method
MP	M^{th}-Order Picard Method
ML	M^{th}-Order Left-Factored Method

SUMMARY

Perhaps one of the most fundamental questions in oceanography is determining the shape of the ocean floor. Most theoretical work done in this area involves using acoustical methods. This research takes a rather different approach. The goal of this research is to determine the shape of the bottom of a body of water using surface measurements such as surface wave measurements. Indeed, methods for this inverse problem can be formulated through the use of the Dirichlet-Neumann operator. As the Dirichlet-Neumann operator is an integral part of the inverse methods, some of this research involves detailing those properties that are required to justify the way it is applied. Specifically the analyticity of the Dirichlet-Neumann operator allows for an expansion of the operator in a series which allows for a straightforward numerical treatment of the methods that will be developed.

The method of proof for establishing the analyticity of the Dirichlet-Neumann operator is motivated by viewing the geometry of the fluid as a perturbation of a system with a flat air-surface interface and a flat bottom boundary, which suggests a double perturbation expansion (one expansion around the top surface, one around the bottom boundary) of the operator might be very useful. A change of variables previous to this expansion allows for the recursive estimation of terms in the expansion. This explicit form of the Dirichelt-Neumann operator presents the ability to design methods that will determine the shape of the bottom deformation, as it now appears explicitly in the operator, though in a genuinely nonlinear way. The methods

developed are simple in execution, but not trivial in nature. Various different order methods will be developed in detail.

The methods developed will be rigorously tested through numerical simulations to test their veracity. A known topography will be given as input to the forward problem which will output surface measurements. Those surface measurements will be used as input data for the inverse methods, whose output will be compared with the original input data. Two different types of representative inputs will be tested. First a small Gaussian bump-like deviation will be introduced, followed by a sandbar type deviation. Not only will the convergence of the methods be tested, but also their range of applicability through variation of parameters that will be used to define the original inputs into the forward problem. Noise will also be added to the input to test the veracity of the methods. These results will then be discussed in detail.

CHAPTER 1

INTRODUCTION

Boundary value and free boundary problems arise in a wide variety of applications in the physical and engineering sciences. From electromagnetics and acoustics (5) to fluid (20) and solid mechanics (13), boundary value and free boundary models are indispensable as a source of quantitative information for real-world phenomena. As important tools for scientists and engineers alike, the analysis (both theoretical and numerical) of these problems is clearly of crucial importance in understanding basic physical processes. While classical problems focus on solving for the field given boundary values, there recently has been much focus on inverse problems. Generally, in an inverse problem one seeks to identify a parameter of the problem which cannot be directly measured given some information about the field which can be measured (and in many problems, some other boundary information as well).

One specific free boundary problem is that of water wave propagation. Surface water wave propagation has long been a subject of study in mathematics. The classical forward problem of wave propagation over variable depth is of great importance in coastal engineering. This problem can be very complex due to the strong presence of shoaling, refraction, diffraction and reflection.

Of no less importance is the ability to detect the shape of the the bottom of the ocean. This problem is also one of oceanography's most challenging problems for both theoretical and practical considerations. On the theoretical side, inverse problems are ill-posed, which will

often cause a direct solution to this (and other similar problems found in a wide array of applied sciences) unobtainable (5). Regularization schemes and filtering are just two common tools to give approximate solutions to inverse problems. From a practical standpoint, the ability to simply go out and take measurements can be difficult, expensive and, at times, even dangerous.

The most widely used method to find the shape of ocean bathymetry is through the detection of acoustic waves which propagate down to the ocean floor and reflect back up to the surface. For a brief sample of recent progress in this enormous field of "Underwater Acoustics" see (27; 4).

This thesis presents a rather different approach to determining the shape of the bottom of the ocean by framing the problem in the setting of a water wave inverse problem. The general water wave inverse problem is stated most simply as trying to ascertain the bottom boundary of a body of water from surface measurements. The methods developed will rely upon *nonlinear* dynamical properties of the *ocean surface* to detect information about the ocean bathymetry. This is very much in the same spirit as (24; 14) who use nonlinear properties of ocean waves to find the bottom shape. Piotrowski and Dugan's (24) method is one among many in the literature which use linear variations in the dispersion relation for shoaling gravity waves as a function of depth to deduce information about the shape of the ocean floor. Grilli (14) has expanded upon these types of methods by taking into account nonlinear contributions to the dispersion relation and achieved remarkable success.

Unlike the methods outlined above, the methods developed in this thesis do not rely solely upon the dispersion relation, rather, the *entire* dynamic water wave problem is utilized. The

Euler equations for an ideal fluid can be reformulated at the surface (28; 10). The Dirichlet–Neumann operator (DNO), also known as the Steklov-Poincaré operator (5), arises as a key component of this reformulation. The DNO produces a first normal derivative (Neumann data) from boundary measurements (Dirichlet data). The DNO plays a crucial role in the proposed methods.

As a prerequisite to using the DNO operator in the inverse methods, certain mathematical properties such as analyticity need to be established. The DNO has found widespread usefulness in a wide range of classical forward problems. For a large sub-class of boundary value and free boundary problems, a simplification and reduction in dimension can be achieved by considering boundary quantities as fundamental variables. This is the case for an ideal fluid flow (20), where the velocity potential must satisfy Laplace's equation. Another example would be linear time-harmonic acoustics (5) where the reduced pressure must satisfy Helmhotz's equation. It is usually possible in situations where the unknown function satisfies a simple differential equation in the interior of the domain problem. In these cases, the field quantity at the surface and, when dealing with a free boundary problem, the shape of the surface usually work as fundamental variables. From these, the value of the field at any point in the domain can be recovered from a suitable integral formula.

Of course, derivatives of the field at the boundary may be of physical interest and/or necessary to correctly pose the physical problem. In this case a challenge arises in producing normal boundary derivatives as these involve, in a fundamental way, the solution of the differential equation on the interior of the problem's domain. For this reason, normal derivative operators

such as the DNO play a key role. Clearly, a detailed understanding of the analytical properties of these DNO is crucial to not only the theoretical study of boundary value and free boundary problems, but also their reliable and accurate numerical simulation.

The first half of this thesis will develop the setting and mathematical properties of the DNO for water waves. Some previous work on the DNO in this setting can be found in (26; 15; 7). This development will include an analyticity result for the setting of free–boundary fluid mechanics over a non-trivial bottom boundary. The result presented will be a specific case of a very general result found in (23). While the proof does not give the sharpest results from a theoretical standpoint (the boundary deformations are only assumed to be C^{s+2}), a more general theoretical result in the case of a flat bottom and arbitrary dimensions can be found in (16). The reason for using a method that does not give the most general results is that the method of proof sets up a stable numerical procedure for simulating the DNO.

The second half of this thesis will detail several methods for solving the water wave inspired inverse problem discussed earlier. These methods rely on an expansion of the DNO in a perturbation series around the bottom boundary. Through this expansion, surprisingly convenient formulas are found that involve the ocean bathymetry. While, not surprisingly, these formulas are ill-conditioned and nonlinear, simple standard techniques from the general theory of inverse problems allows for an accurate approximation of the bottom topography.

The methods developed will then be rigorously tested. A known bottom topography will be used as data for the forward problem to generate wave data. This data will then be used as input for the inverse methods, whose output can then be compared to the original known

topography. Several parameters will be varied to see how well the different methods respond to bottom topographies of various shapes and sizes. Lastly noise of various magnitude will be added to the wave data, to show that the methods will work when measurement errors are introduced.

CHAPTER 2

THE EQUATIONS OF MOTION

This chapter will focus on the theoretical foundation and the motivation for the inverse problem that will be proposed and dealt with in later chapters. A proper starting point for any problem that finds its motivation from fluid mechanics is the famous Navier-Stokes equations. After outlining some assumptions, a system of equations will be developed which describe the movement of water waves over a non-trivial bottom boundary. This system of equations can be written as Hamiltonian system that allows a surface reformulation of the evolution equations. In this development arises the Dirichlet-Neumann operator, which forms the basis for the rest of the thesis.

2.1 Navier-Stokes Equations

The familiar Navier-Stokes equations describe water wave movement for an incompressible Newtonian fluid:

$$\partial_t \mathbf{u} + (\mathbf{u} \cdot \nabla)\mathbf{u} = -\frac{1}{\rho}\nabla p + \nu \Delta \mathbf{u} + g \tag{2.1a}$$

$$\nabla \cdot \mathbf{u} = 0, \tag{2.1b}$$

where $\mathbf{u}$ is the velocity vector, ρ is the density of the fluid, p is the pressure, g is the gravitational force and ν is the viscosity. For the purposes of this thesis, the fluid will also be assumed to be inviscid, so that, from this point forward, $\nu = 0$. One last assumption will be made about

the fluid itself, and that is it also be irrotational ($\nabla \times \mathbf{u} = 0$). A fluid assigned these three characteristics (incompressible, inviscid, irrotational) is typically referred to as an ideal fluid. Irrotationality leads to the existence of a velocity potential φ where $\mathbf{u} = \nabla\varphi$. Substituting this expression into Equation 2.1b, implies that the velocity potential φ satisfies Laplace's equation $\Delta\varphi = 0$ throughout the fluid's domain.

The Navier-Stokes equations form the backbone of most fluid dynamics. While by no means an exhaustive list, some applications of the Navier-Stokes equation include the movement of air around an aerofoil, the movement of a very viscous liquid, as well as surface water waves. Maybe the most critical aspect to specifying the intended application of Equation 2.1 is to specify the domain that the fluid occupies. The fluid domain with a non-flat, impenetrable bottom boundary with a free surface as its upper boundary consists of the region

$$S_{h,\zeta,\eta} = \{(x,y)|(x,y) \in \mathbb{R}^{d-1} \times \mathbb{R}, -h + \zeta(x) < y < \eta(x,t)\}, \tag{2.2}$$

where $\eta(x,t)$ specifies the moving air/fluid interface, h is a fixed depth, $\zeta(x)$ is the deviation of the bottom topography from the fixed depth. To clarify, $d = 2$ in the case of one horizontal variable and $d = 3$ in the case of 2 horizontal variables. For the theoretical aspects of this thesis (the bulk of chapters 2-4) $d = 3$ (the theory can generalize to higher dimensions as well), while the chapter on a water wave inspired inverse problem will use $d = 2$ for computational purposes.

Without going through their detailed development, which can be found in any fluid mechanics book (20; 1), the boundary conditions used for this domain are the typical kinematic and Bernoulli conditions on the free surface $y = \eta(x,t)$:

$$\partial_t \eta = \partial_y \varphi - \nabla_x \eta \cdot \nabla_x \varphi, \qquad \partial_t \varphi = -g\eta - \frac{1}{2}|\nabla \varphi|^2, \tag{2.3}$$

respectively. At $y = -h + \zeta(x)$, the boundary condition is derived from the property of impenetrability–that the fluid can not cross the bottom boundary. This implies that the normal derivative of the velocity potential at the bottom boundary should be zero, i.e. $\partial_y \varphi - \nabla_x \zeta \cdot \nabla_x \varphi = 0$. For simplicity there will be an additional assumption of periodic boundary conditions with respect to the lattice $\Gamma \subset \mathbb{R}^{d-1}$ giving period cell $P(\Gamma)$ and wavenumbers in the conjugate lattice Γ'. For convenience, the classical Euler equations that define the movement of an ideal fluid are collected below.

$$\Delta \varphi = 0 \qquad \text{in } S_{h,\zeta,\eta} \tag{2.4a}$$

$$\partial_t \eta - \partial_y \varphi + \nabla_x \eta \cdot \nabla_x \varphi = 0 \qquad \text{on } y = \eta(x,t) \tag{2.4b}$$

$$\partial_t \varphi + g\eta + \frac{1}{2}|\nabla \varphi|^2 = 0 \qquad \text{on } y = \eta(x,t) \tag{2.4c}$$

$$\partial_y \varphi - \nabla_x \zeta \cdot \nabla_x \varphi = 0 \qquad \text{on } y = -h + \zeta(x). \tag{2.4d}$$

2.2 Zakharov's Hamiltonian Formulation

Zakharov, in his famous paper (28), was able to write these equations in a Hamiltonian system in the canonical variables $(\eta(x,t), \xi(x,t))$, where $\xi(x,t)$ is defined to be the value of

the velocity potential at the surface $y = \eta(x,t)$, i.e. $\xi(x,t) = \varphi(x,\eta(x,t),t)$. The evolution equations then take the form of the Hamiltonian system

$$\partial_t \begin{pmatrix} \eta \\ \xi \end{pmatrix} = \begin{pmatrix} 0 & I \\ -I & 0 \end{pmatrix} \begin{pmatrix} \delta_\eta H \\ \delta_\xi H \end{pmatrix}, \tag{2.5}$$

where H is the Hamiltonian functional

$$H = \int \int_{-h+\zeta}^{\eta} \frac{1}{2}|\nabla\varphi|^2 dy dx + \int \frac{1}{2} g\eta^2 dx \tag{2.6}$$

2.3 Surface Reformulation

The Hamiltonian formulation Equation 2.6 and the solvability of Laplace's equation on the domain $S_{h,\zeta,\eta}$ given ξ, leads to a reformulation of Equation 2.4 at the surface (10). The development of these equations will be detailed in Chapter 4. Crucial to this reformulation is the Dirichlet–Neumann operator (DNO), $G(\eta,\zeta)\xi$, which also allows the Hamiltonian Equation 2.6 to be rewritten as

$$H = \int \frac{1}{2}\xi G(\eta,\zeta)[\xi] dx + \int \frac{1}{2} g\eta^2 dx. \tag{2.7}$$

The DNO is so named because it takes Dirichlet data, $\xi(x)$, as input and outputs Neumann data, $\partial_n\varphi$. More specifically the DNO expresses the normal derivative of φ at the surface η in terms of ξ and the domain $S_{h,\zeta,\eta}$.

Inspired by the geometry of the Euler equations Equation 2.4, and through the surface reformulation of Craig and Sulem, we study the DNO and its associated boundary value problem,

$$\Delta v = 0 \qquad \text{in } S_{h,\zeta,\eta} \tag{2.8a}$$

$$\partial_y v - \nabla_x \zeta \cdot \nabla_x v = 0 \qquad \text{on } y = -h + \zeta(x) \tag{2.8b}$$

$$v(x, \eta(x)) = \xi(x) \tag{2.8c}$$

$$\varphi(x + \gamma, y) = \varphi(x, y) \qquad \text{for all } \gamma \in \Gamma. \tag{2.8d}$$

Given the intuitive definition of the DNO and finding a solution of Equation 2.8, the DNO is defined as

$$G(\eta, \zeta)\xi = \partial_y v - \nabla_x \eta \cdot \nabla_x v|_{y=\eta}. \tag{2.9}$$

As the DNO is crucial to the surface reformulation, it is imperative that its mathematical properties are properly understood. The highly implicit nature of the DNO can make this difficult. An explicit form for the DNO helps simplify things greatly. The next chapter will discuss this in detail.

CHAPTER 3

THE DIRICHLET-NEUMANN OPERATOR

As was described briefly in the previous chapter, the system of equations Equation 2.8 can be written in terms of the canonical variables ξ and η. Crucial to this process is the DNO, an implicit operator that acts on ξ. Being able to accurately compute the DNO is very important, not only to the theoretical study of boundary value and free boundary problems, but also in forming reliable numerical models of these problems.

One method that allows for an accurate numerical approximation of the DNO is a perturbation expansion. The DNO is often exactly solvable in the case of simple geometries. If $S_{h,\zeta,\eta}$ is viewed as a perturbation of a geometry with flat upper and lower boundaries $S_{h,0,0}$, then a double perturbation expansion, in powers of η and ζ, of the DNO is appealing. While there are several methods that develop this expansion into a numerically convenient form, only one such method also leads to a straightforward inductive proof of analyticity. In this chapter, certain methods for expansion will be developed, and an analyticity theorem will be detailed.

3.1 Expansion

From the definition of the DNO, Equation 2.9, one can see that it is highly implicit in nature. For certain geometries, however, it can be explicitly found. Such is the case when the water surface and bottom boundary are uniformly flat, i.e. when $\eta = 0$ and $\zeta = 0$. In this case, we can calculate the DNO:

$$\begin{aligned} G(\eta,\zeta)\xi(x) &= \nabla v(x,\eta(x))\cdot(-\nabla_x\eta,1)^T \\ &= \partial_y v(x,0). \end{aligned} \tag{3.1}$$

In this case, the solution of Equation 2.8 is given by

$$v(x,y) = \sum_{k\in\Gamma'} \frac{\cosh(|k|(y+h))}{\cosh(|k|h)}\hat{\xi}_k e^{ik\cdot x}, \tag{3.2}$$

where $\hat{\xi}_k$ are the Fourier coefficients of $\xi(x)$. Then by substituting Equation 3.2 into Equation 3.1, it is easily seen that applying the DNO to $\xi(x) = v(x,0)$ results in

$$\begin{aligned} G(0,0)\xi(x) = \partial_y v(x,0) &= \sum_{k\in\Gamma'} |k|\tanh(|k|h)\hat{\xi}_k e^{ik\cdot x} \\ &= |D|\tanh(h|D|)\xi(x), \end{aligned} \tag{3.3}$$

where $D = -i\nabla_x$. This, of course, implies that $G(0,0) = |D|\tanh(h|D|)$.

Given that finding an explicit formula for the DNO is so simple in such a geometry, a double perturbative approach seems to suggest itself as a plausible way to calculate the DNO. In this approach the general surfaces $y = \eta$ and $y = -h + \zeta$ are viewed as perturbations from the planes $y = 0$ and $y = -h$, and an explicit expression for the DNO may be found by writing it in a double perturbation series about the unperturbed surfaces. Letting $\eta(x) = \varepsilon f(x)$ and $\zeta(x) = \delta b(x)$, where ε and δ are viewed as small parameters, we wish to write

$$G(\eta,\zeta)\xi = \sum_{n=0}^{\infty}\sum_{m=0}^{\infty} G_{n,m}(f,b)[\xi]\delta^m\varepsilon^n \tag{3.4}$$

There have been many papers that discuss such an approach in the case of a flat bottom boundary ($\zeta(x) = 0$) (3; 10; 25; 21; 8; 22) and more recently in the case of a nontrivial bottom boundary (26; 15; 7; 23).

3.2 Field Expansion and Operator Expansion

There are several ways to derive formulas for the $G_{n,m}$ in the expansion of the DNO. One way, termed "Field Expansions" (FE), expands the field in a double perturbation series

$$v(x, y; \varepsilon, \delta) = \sum_{n=0}^{\infty}\sum_{m=0}^{\infty} v_{n,m}(x, y)\delta^m\varepsilon^n, \tag{3.5}$$

where the δ and ε come from the substitutions $\eta(x) = \varepsilon f(x)$ and $\zeta(x) = \delta b(x)$. The $v_{n,m}(x, y)$ can be recursively solved for by solving a system of equations for each pair (n, m). Those explicit solutions for the $v_{n,m}$ can then can be used when Equation 3.5 is substituted into the definition of the DNO (Equation 2.9) to solve for the $G_{n,m}(f, b)$.

To solve for the $v_{n,m}(x, y)$ we will make use of two separate Taylor expansions of $v(x, y; \varepsilon, \delta)$. One expansion will be about the surface $y = 0$: $v(x, \varepsilon f(x)) = \sum_l \partial_y^l v(x, 0)\frac{f^l}{l!}\varepsilon^l$, and one about the bottom $y = -h$: $v(x, -h + \delta b(x)) = \sum_l \partial_y^l v(x, -h)\frac{b^l}{l!}\delta^l$. Substituting Equation 3.5 into these expansions results in

$$v(x, \varepsilon f(x)) = \sum_{l=0}^{\infty}\sum_{n=0}^{\infty}\sum_{m=0}^{\infty} \partial_y^l v_{n,m}(x, 0)\frac{f^l}{l!}\varepsilon^{l+n}\delta^m \tag{3.6a}$$

$$v(x, -h + \delta b(x)) = \sum_{l=0}^{\infty}\sum_{n=0}^{\infty}\sum_{m=0}^{\infty} \partial_y^l v_{n,m}(x, -h)\frac{b^l}{l!}\varepsilon^n\delta^{l+m}. \tag{3.6b}$$

Then substituting Equation 3.5 into Equation 2.8a, and Equation 3.6a,b into their respective boundary conditions (Equation 2.8b,c), it can be shown that the $v_{n,m}$ must satisfy

$$\Delta v_{n,m} = 0, \qquad \text{in } S_{h,0,0} \tag{3.7a}$$

$$v_{n,m}(x,0) = H^{(1)}_{n,m}(x) \tag{3.7b}$$

$$\partial_y v_{n,m}(x,-h) = H^{(2)}_{n,m}(x) \tag{3.7c}$$

$$v_{n,m}(x+\gamma,y) = v_{n,m}(x,y), \qquad \text{for all } \gamma \in \Gamma. \tag{3.7d}$$

where

$$H^{(1)}_{n,m}(x) = \bar{\delta}_{n,0}\bar{\delta}_{m,0}\xi(x) - \sum_{l=1}^{n} \frac{f^l}{l!}\partial_y^l v_{n-l,m}(x,0) \tag{3.8}$$

$$\begin{aligned} H^{(2)}_{n,m}(x) = {} & \nabla_x b \cdot \sum_{l=0}^{m-1} \frac{b^l}{l!}\nabla_x \left[\partial_y^l v_{n,m-l-1}(x,-h)\right] \\ & - \sum_{l=1}^{m} \frac{b^l}{l!}\partial_y^{l+1} v_{n,m-l}(x,-h), \end{aligned} \tag{3.9}$$

and $\bar{\delta}_{j,k}$ is the Kronecker delta. This system of equations is solved by using the general spectral representation of the solution, and solving for the coefficients using the boundary conditions. While the form of $v_{0,0}$ from Equation 3.2, $v_{0,0}(x,y) = \sum_{k\in\Gamma'} \frac{\cosh(|k|(y+h))}{\cosh(|k|h)}\hat{\xi}_k e^{ik\cdot x}$, suggests using a spectral solution involving $\cosh(|k|(y+h))$ and $\sinh(|k|(y+h))$, it is most convenient, for $(n,m) \neq (0,0)$, to use the form

$$v_{n,m}(x,y) = \sum_{k\in\Gamma'} \left[\cosh(|k|y)s_{n,m,k} + \sinh(|k|y)t_{n,m,k}\right] e^{ik\cdot x}, \tag{3.10}$$

where $s_{n,m,k}$ and $t_{n,m,k}$ are Fourier coefficients. Then using the spectral representations in Equation 3.7b and Equation 3.7c, we get a system of equations in which we can solve for the Fourier coefficients in Equation 3.10. To be exact, if $H^{(j)}_{n,m}(x) = \sum_{k\in\Gamma'} \hat{H}^{(j)}_{n,m,k} e^{ik\cdot x}$ for $j = 1, 2$, then

$$s_{n,m,k} = \hat{H}^{(1)}_{n,m,k} \tag{3.11a}$$

$$t_{n,m,k} = \tanh(h|k|)\hat{H}^{(1)}_{n,m,k} + \frac{1}{|k|\cosh(h|k|)}\hat{H}^{(2)}_{n,m,k}. \tag{3.11b}$$

These formulas can be used recursively to find formulas for the Fourier coefficients. Once the formulas for $v_{n,m}$ are found, the $G_{n,m}$ can be calculated. Using a process similar to the one which recovered Equation 3.7 from Equation 2.8, the DNO can be written as

$$G_{n,m}(f,b)\xi = \sum_{l=0}^{n} \frac{f^l}{l!}\partial_y^{l+1} v_{n-l,m}(x,0) - \nabla_x f \sum_{l=0}^{n-1} \frac{f^l}{l!}\nabla_x \partial_y^l v_{n-l-1,m}(x,0). \tag{3.12}$$

To clearly illustrate this method, $G_{1,0}$ and $G_{0,1}$ will be explicitly calculated. From Equation 3.12, we see that to get the formula for $G_{1,0}$, the spectral solution $v_{1,0}$ must be found. Inserting Equation 3.10 for $v_{1,0}$ into the boundary conditions Equation 3.7b,c, results in

$$\begin{aligned}\sum_{k\in\Gamma'} s_{1,0,k}\hat{\xi}_k e^{ik\cdot x} &= -f(x)\partial_y v_{0,0}(x,0) \\ &= -f(x)\sum_{k\in\Gamma'} |k|\tanh(h|k|)\hat{\xi}_k e^{ik\cdot x}\end{aligned} \tag{3.13a}$$

$$\sum_{k\in\Gamma'} \Big[|k|\cosh(h|k|)t_{1,0,k} - |k|\sinh(h|k|)s_{1,0,k}\Big]\hat{\xi}_k e^{ik\cdot x} = 0. \tag{3.13b}$$

This system of equations can be solved for $s_{1,0,k}$ and $t_{1,0,k}$. At this point, we use the more convenient "Fourier multiplier" notation which identifies k to D just as the operator $-i\nabla_x$ was written as D earlier when writing the formula for $G_{0,0}$. With this in mind, the spectral solution takes the form

$$v_{n,m}(x,y) = \left[\cosh(|D|y)S_{n,m} + \sinh(|D|y)T_{n,m}\right]\xi(x), \tag{3.14}$$

and Equation 3.13a,b become

$$S_{1,0}\xi = -f(x)|D|\tanh(h|D|)\xi \tag{3.15a}$$

$$T_{1,0}\xi = \frac{|D|\sinh(h|D|)}{|D|\cosh(h|D|)}S_{1,0}\xi. \tag{3.15b}$$

Therefore,

$$S_{1,0} = -f|D|\tanh(h|D|), \tag{3.16a}$$

$$T_{1,0} = -\tanh(h|D|)f|D|\tanh(h|D|). \tag{3.16b}$$

This leads to the solution

$$\begin{aligned} v_{1,0}(x,y) = -\Big[&\cosh(|D|y)f(x)|D|\tanh(h|D|) \\ &+ \sinh(|D|y)\tanh(h|D|)f(x)|D|\tanh(h|D|)\Big]\xi(x), \end{aligned} \tag{3.17}$$

which can then be used to calculate $G_{1,0}$. From Equation 3.12,

$$\begin{aligned} G_{1,0}(f,b)\xi(x) &= \partial_y v_{1,0}(x,0) - \nabla_x f(x)\cdot\nabla_x v_{0,0}(x,0) \\ &= -|D|\tanh(h|D|)f(x)|D|\tanh(h|D|)\xi(x) + Df(x)\cdot D\xi(x). \end{aligned} \tag{3.18}$$

So

$$\begin{aligned} G_{1,0}(f,b) &= DfD - |D|\tanh(h|D|)f|D|\tanh(h|D|) \\ &= Df\cdot D - G_{0,0}fG_{0,0}. \end{aligned} \tag{3.19}$$

Similarly for $G_{0,1}$, the spectral solution for $v_{0,1}$ needs to be found. When Equation 3.10 for $v_{1,0}$ is inserted into Equation 3.7b, this results in

$$\sum_{k\in\Gamma'} s_{0,1,k}\hat{\xi}_k e^{ik\cdot x} = 0, \tag{3.20a}$$

implying that, $s_{0,1,k} = 0$. So that from Equation 3.7c (using Fourier multipliers),

$$\begin{aligned} |D|\cosh(h|D|)T_{0,1}\xi &= -(Db(x))\cdot(Dv_{0,0}(x,-h)) - b(x)\partial_y^2 v_{0,0}(x,-h) \\ &= -(Db(x))\cdot(D\mathrm{sech}(h|D|)\xi) - b(x)|D|^2\mathrm{sech}(h|D|)\xi \\ &= -D\cdot b(x)D\mathrm{sech}(h|D|)\xi, \end{aligned} \tag{3.20b}$$

where we have used the fact that $|D|^2 = D^2$, and the product rule: $(Db(x))\cdot(X(x)) + b(x)D^2(X(x)) = D\cdot bDX(x)$. Therefore,

$$T_{0,1} = -\frac{D}{|D|}\mathrm{sech}(h|D|)\cdot b(x)D\mathrm{sech}(h|D|), \tag{3.21}$$

which leads to

$$v_{0,1}(x,y) = -\sinh(|D|y)\frac{D}{|D|}\text{sech}(h|D|)\cdot b(x)D\text{sech}(h|D|)\xi(x). \tag{3.22}$$

And $G_{1,0}$ can be calculated,

$$G_{0,1}(f,b)\xi(x) = -D\text{sech}(h|D|)\cdot b(x)D\text{sech}(h|D|)\xi(x). \tag{3.23}$$

Up to this point then, the following terms of the expansion of the DNO have been calculated.

$$G_{0,0}(f,b) = |D|\tanh(h|D|) \tag{3.24a}$$

$$G_{1,0}(f,b) = Df\cdot D - G_{0,0}fG_{0,0} \tag{3.24b}$$

$$G_{0,1}(f,b) = -D\text{sech}(hD)\cdot bD\text{sech}(hD). \tag{3.24c}$$

Another method for finding the $G_{n,m}$ substitutes the double sum form for the DNO from Equation 3.4 directly into the definition of the DNO Equation 2.9. This method is termed "Operator Expansion" (OE), as the main expansion is done on the operator and not the field. OE will be outlined in more detail in the next chapter.

These two methods have much computational value (10; 15), but their usefulness in analyzing the mathematical properties of the DNO such as analyticity is found lacking. While the results in (22) show that this series converges in the case of $\zeta(x) = 0$, and an extension of those results for when $\zeta(x) \neq 0$ certainly is expected, there is a seeming contradiction. The process of calculating the series makes evident a seemingly strong requirement that both profiles η and

ζ have a high degree of regularity. On the other hand, the smoothness requirements of these analyticity results is much less restricted (they need only be a C^1 perturbation of a plane) (9; 8). This seeming contradiction can be explained through cancelations that occur in this expansion. These cancelations and the effects that they have on numerical simulations are outlined in (21)

A third method, while not as straightforward in its derivation as FE and OE, is very useful for proving analyticity properties of the DNO. This method is called "Transformed Field Expansions" (TFE). In this method, the field undergoes a non-conformal transformation, and then expanded. This method will be outlined in detail in the next section.

3.3 The Transformed Field Expansion

As mentioned above, the first step for TFE is to make a non-conformal transformation of the field. The motivation for this transformation is to map the domain $S_{h,\zeta,\eta}$ into a domain consisting of a simple, separable geometry. The change of variables is given by

$$x' = x, \qquad y' = \frac{h(y-\eta)}{h-\zeta+\eta}. \tag{3.25}$$

Note then that $y = y'(h-\zeta+\eta)/h+\eta$. This transformation maps our domain $S_{h,\zeta,\eta}$ into the domain $S_{h,0,0}$ or equivalently it maps $y = \eta \rightarrow y' = 0$ and $y = -h+\zeta \rightarrow y' = -h$. This change of variables also transforms v into

$$u(x',y') = v(x', y'(h-\zeta+\eta)/h+\eta). \tag{3.26}$$

With this change of variables, the system of equations Equation 2.8 also needs to transformed. To simplify the transformation into the system of equations in the new coordinate system, the following functions become very useful.

$$M(x') := (h - \zeta(x') + \eta(x')) \tag{3.27}$$

$$\tilde{M}(x') := M(x') - h = \eta(x') - \zeta(x') \tag{3.28}$$

$$N(x', y') := -(y' + h)\nabla_x \eta(x') + y'\nabla_x \zeta(x'). \tag{3.29}$$

These functions lead to the formulas

$$\partial_{y'} N = -\nabla_{x'} M \tag{3.30a}$$

$$M\nabla_x = M\nabla_{x'} + N\partial_{y'} \tag{3.30b}$$

$$M\partial_y = h\partial_{y'} \tag{3.30c}$$

$$M\mathrm{div}_{x'}[\cdot] = M\mathrm{div}_{x'}[\cdot] + N\partial_{y'}[\cdot]. \tag{3.30d}$$

With these preliminary calculations, we are ready to completely reformulate Equation 2.8 in the new coordinate system. To simplify the process it will be convenient to multiply both sides of Laplace's equation by M^2. While it is certainly possible to formulate the system of equations in this new coordinate system without this multiplication, quotients appear on the right hand side in $\zeta(x')$ and $\eta(x')$, which are not only inconvenient for the proof of analyticity, but also not optimal for a numerical implementation of the expansion.

$$
\begin{aligned}
M^2\Delta v &= M^2\mathrm{div}_x(\nabla_x v) + M^2\partial_y^2 v \\
&= M\mathrm{div}_x(M\nabla_x v) - \nabla_x M\cdot(M\nabla_x v) + M\partial_y(M\partial_y v) \\
&= (M\mathrm{div}_{x'} + N\partial_{y'})(M\nabla_{x'}u + N\partial_{y'}u) - M\nabla_{x'}M\cdot\nabla_{x'}u \\
&\qquad - N\cdot\nabla_{x'}M\partial_{y'}u + h^2\partial_{y'}^2 u \\
&= M\mathrm{div}_{x'}(M\nabla_{x'}u) + M\mathrm{div}_{x'}(N\partial_{y'}u) + N\cdot\partial_{y'}(M\nabla_{x'}u) \\
&\qquad + N\cdot\partial_{y'}(N\partial_{y'}u) - M\nabla_{x'}M\cdot\nabla_{x'}u - N\cdot\nabla_{x'}M\partial_{y'}u + h^2\partial_{y'}^2 u \\
&= h\mathrm{div}_{x'}(M\nabla_{x'}u) + \tilde{M}\mathrm{div}_{x'}(M\nabla_{x'}u) + \mathrm{div}_{x'}(MN\partial_{y'}u) \\
&\qquad - \nabla_{x'}M\cdot N\partial_{y'}u + \partial_{y'}(N\cdot M\nabla_{x'}u) - \partial_{y'}N\cdot(M\nabla_{x'}u) \\
&\qquad + \partial_{y'}(|N|^2\partial_{y'}u) - \partial_{y'}N\cdot N\partial_{y'}u - M\nabla_{x'}M\cdot\nabla_{x'}u - N\cdot\nabla_{x'}M\partial_{y'}u + h^2\partial_{y'}^2 u \\
&= h^2\Delta' u + \mathrm{div}_{x'}((2h\tilde{M}+\tilde{M}^2)\nabla_{x'}u + NM\partial_{y'}u) + \partial_{y'}(N\cdot M\nabla_{x'}u + |N|^2\partial_{y'}u) \\
&\qquad - \nabla_{x'}\tilde{M}\cdot(M\nabla_{x'}u) - N\cdot\nabla_{x'}M\partial_{y'}u.
\end{aligned}
$$

Then, since $\Delta v = 0$,

$$
\begin{aligned}
h^2\Delta' u = \mathrm{div}_{x'}\left[-(\tilde{M}^2+2h\tilde{M})\nabla_{x'}u - NM\partial_{y'}u\right] - \partial_{y'}\left[N\cdot M\nabla_{x'}u + |N|^2\partial_{y'}u\right] \\
+ \left[M\nabla_{x'}M\cdot\nabla_{x'}u + N\cdot\nabla_{x'}M\partial_{y'}u\right]. \quad (3.31)
\end{aligned}
$$

Likewise, to find the bottom boundary condition, we solve Equation 2.8b for $\partial_y v$ and multiply both sides by M resulting in (note that $N(x', -h + \zeta(x')) = -h\nabla_{x'}\zeta(x')$)

$$\begin{aligned} M\partial_y v(x, -h + \zeta(x)) &= M\nabla_x \zeta \cdot \nabla_x u(x, -h) \\ &= \nabla_{x'}\zeta(x') \cdot \left[M\nabla_{x'} u(x, -h) - h\nabla_{x'}\zeta(x')\partial_{y'} u(x', -h)\right] \\ &= M\nabla_{x'}\zeta(x') \cdot \nabla_{x'} u(x', -h) - h|\nabla_{x'}\zeta(x')|^2 \partial_{y'} u(x', -h), \end{aligned} \tag{3.32}$$

which implies that

$$h\partial_{y'} u(x, -h) = M\nabla_x \zeta(x') \cdot \nabla_{x'} u(x, -h) - h|\nabla_x \zeta(x')|^2 \partial_{y'} u(x, -h). \tag{3.33}$$

The DNO is transformed to

$$\begin{aligned} MG(\eta, \zeta)\xi(x) &= M\partial_y v(x, \eta(x)) - M\nabla_x \eta(x) \cdot \nabla_x v(x, \eta(x)) \\ &= h\partial_{y'} u(x', 0) - \nabla_{x'}\eta(x') \cdot \left[M\nabla_{x'} u(x', 0) + N(x', 0)\partial_{y'} u(x', 0)\right] \\ &= h(1 + |\nabla_{x'}\eta(x')|^2)\partial_{y'} u(x', 0) - M\nabla_{x'}\eta(x') \cdot \nabla_{x'} u(x', 0). \end{aligned} \tag{3.34}$$

Remark 3.3.1. *To simplify the appearance of some of the expressions to follow, $u_{n,m}$ may refer to $u_{n,m}(x', 0)$, $u_{n,m}(x', y')$ or $u_{n,m}(x, -h)$. The context should give clarity. In the previous expression Equation 3.34, it would have been clear that $u_{n,m}$ would be meant as $u_{n,m}(x', 0)$ as the DNO is defined on the surface $y = 0$. The notation will be clarified when the context might be unclear.*

Upon dropping the primes, our system of equations can be written in the convenient divergence form

$$\Delta u = \mathrm{div}_x F^{(1)}(x,y) + \partial_y F^{(2)}(x,y) + F^{(3)}(x,y) \tag{3.35a}$$

$$u(x,0) = \xi(x) \tag{3.35b}$$

$$\partial_y u(x,-h) = J(x) \tag{3.35c}$$

$$u(x,y) = u(x+\gamma,y) \qquad \text{for all } \gamma \in \Gamma, \tag{3.35d}$$

where

$$h^2 F^{(1)} = -(2h\tilde{M} + \tilde{M}^2)\nabla_x u - NM\partial_y u \tag{3.36a}$$

$$h^2 F^{(2)} = -MN \cdot \nabla_x u - |N|^2 \partial_y u \tag{3.36b}$$

$$h^2 F^{(3)} = M\nabla_x M \cdot \nabla_x u + N \cdot \nabla_x M \partial_y u \tag{3.36c}$$

$$hJ(x) = M\nabla_x \zeta(x) \cdot \nabla_x u(x,-h) - h|\nabla_x \zeta(x)|^2 \partial_y u(x,-h). \tag{3.36d}$$

Now that Equation 2.8 have been rewritten in the new coordinate system, the field and the DNO are expanded as was done in the previous methods. Letting $\eta(x) = \varepsilon f(x)$ and $\zeta(x) = \delta b(x)$, the following expansions are formally made:

$$u(x,y;\varepsilon,\delta) = \sum_{n=0}^{\infty}\sum_{m=0}^{\infty} u_{n,m}(x,y)\delta^m \varepsilon^n, \tag{3.37}$$

and

$$G(\varepsilon f, \delta b)\xi = \sum_{n=0}^{\infty}\sum_{m=0}^{\infty} G_{n,m}(f,b)\xi\delta^m\varepsilon^n. \tag{3.38}$$

The system of equations for each $u_{n,m}$, which can be solved recursively, now need to be identified. Inserting Equation 3.37 into Equation 3.35, the system of equations for each $u_{n,m}$ is found by equating terms of like order in δ and ε. The system at order $(n,m) = (0,0)$ becomes

$$\Delta u_{0,0} = 0 \tag{3.39a}$$

$$u_{0,0}(x,0) = \xi(x) \tag{3.39b}$$

$$\partial_y u_{0,0}(x,-h) = 0 \tag{3.39c}$$

$$u_{0,0}(x+\gamma, y) = u_{0,0}(x,y) \qquad \forall\ \gamma \in \Gamma. \tag{3.39d}$$

For $n+m > 0$ the system becomes

$$\Delta u_{n,m} = \mathrm{div}_x F^{(1)}_{n,m}(x,y) + \partial_y F^{(2)}_{n,m}(x,y) + F^{(3)}_{n,m}(x,y) \tag{3.40a}$$

$$u_{n,m}(x,0) = 0 \tag{3.40b}$$

$$\partial_y u_{n,m}(x,-h) = J_{n,m}(x) \tag{3.40c}$$

$$u_{n,m}(x+\gamma, y) = u_{n,m}(x,y) \qquad \forall\ \gamma \in \Gamma. \tag{3.40d}$$

Formulas for $F^{(j)}_{n,m}(x,y)$ $(j=1,2,3)$ and $J_{n,m}(x,y)$ are derived from substituting Equation 3.37 and Equation 3.36 into Equation 3.35 and matching terms of of the same order. This leads to the formulas

$$\begin{aligned}
h^2F^{(1)}_{n,m} &= h(2b\nabla_x - y\nabla_x b\partial_y)u_{n,m-1} \\
&\quad - h(2f\nabla_x - (y+h)\nabla_x f\partial_y)u_{n-1,m} \\
&\quad - (b^2\nabla_x + (y/2)\nabla_x(b^2)\partial_y)u_{n,m-2} \\
&\quad - (f^2\nabla_x + (y+h)/2\nabla_x(f^2)\partial_y)u_{n-2,m} \\
&\quad + (2bf\nabla_x - ((y+h)b\nabla_x f - yf\nabla_x b)\partial_y)u_{n-1,m-1},
\end{aligned} \tag{3.41a}$$

$$\begin{aligned}
h^2F^{(2)}_{n,m} &= -hy\nabla_x b\cdot\nabla_x u_{n,m-1} \\
&\quad + h(y+h)\nabla_x f\cdot\nabla_x u_{n-1,m} \\
&\quad + (y/2\nabla_x(b^2)\cdot\nabla_x - y^2|\nabla_x b|^2\partial_y)u_{n,m-2} \\
&\quad + ((y+h)/2\nabla_x(f^2)\cdot\nabla_x - (y+h)^2|\nabla_x f|^2\partial_y)u_{n-2,m} \\
&\quad - \left[((y+h)b\nabla_x f + yf\nabla_x b)\nabla_x - 2(y+h)y\nabla_x f\cdot\nabla_x b\partial_y\right]u_{n-1,m-1},
\end{aligned} \tag{3.41b}$$

$$\begin{aligned}
h^2F^{(3)}_{n,m} &= -h\nabla_x b\cdot\nabla_x u_{n,m-1} + h\nabla_x f\cdot\nabla_x u_{n-1,m} \\
&\quad + (1/2\nabla_x(b^2)\cdot\nabla_x - y|\nabla_x b|^2\partial_y)u_{n,m-2} \\
&\quad + (1/2\nabla_x(f^2)\cdot\nabla_x - (y+h)|\nabla_x f|^2\partial_y)u_{n-2,m} \\
&\quad + (-\nabla_x(fb)\nabla_x + (2y+h)\nabla_x f\cdot\nabla_x b\partial_y)u_{n-1,m-1},
\end{aligned} \tag{3.41c}$$

$$hJ_{n,m} = h\nabla_x b \cdot \nabla_x u_{n,m-1} - b\nabla_x b \cdot \nabla_x u_{n,m-2} + f\nabla_x b \cdot \nabla_x u_{n-1,m-1} - h|\nabla_x b|^2 \partial_y u_{n,m-2}. \tag{3.41d}$$

Once the solutions $u_{n,m}$ have been found, the DNO can be explicitly calculated. Inserting both Equation 3.37 and Equation 3.38 into Equation 3.34 and collecting terms of the same order the formulas for the $G_{n,m}$ can be found:

$$G_{n,m}(f,b)\xi = -h^{-1}\nabla_x f \cdot (h\nabla_x u_{n-1,m} - b\nabla_x u_{n-1,m-1} + f\nabla_x u_{n-2,m}) + \partial_y u_{n,m} + |\nabla_x f|^2 \partial_y u_{n-2,m} + fG_{n-1,m}(f,b)\xi + bG_{n,m-1}(f,b)\xi. \tag{3.42}$$

From the above expression, it is seen that getting a bound on the $G_{n,m}$ is connected to getting bounds on $u_{n,m}$ and some of it's "precursors". More technically, the analyticity of the DNO is a direct result of the analyticity of the field.

3.4 Analyticity of the DNO

Before proving an analyticity property for the DNO, some norms that will be used throughout this chapter should be introduced. If f is a function of only x, g is a function of only y and h is a function of x and y, then their respective Sobolev type norms are defined by

$$\begin{aligned}
\|f\|^2_{H^s(P(\Gamma))} &= \sum_{k\in\Gamma'} |\hat{f}(k)|^2\langle k\rangle^{2s} \\
\|g\|^2_{H^s([-h,0])} &= \sum_{l=0}^{s}\int_{-h}^{0} |\partial_y^l g(y)|^2 dy \\
\|h\|^2_{H^s(P(\Gamma)\times[-h,0])} &= \sum_{l=0}^{s}\sum_{k\in\Gamma'}\int_{-h}^{0} |\partial_y^l \hat{g}(k,y)|^2 dy\langle k\rangle^{2(s-l)},
\end{aligned}$$

where $\langle k\rangle = \sqrt{1+|k|^2}$. There will also be repeated use of the following algebra estimates (2),

$$\begin{aligned}
\|\mu h\|_{H^s} &\leq C(s)|\mu|_{C^s}\|h\|_{H^s} \\
\|\mu h\|_{H^{s+1/2}} &\leq C(s+1/2)|\mu|_{C^{s+1/2+\alpha}}\|h\|_{H^{s+1/2}},
\end{aligned}$$

where C^s is a classical Hölder space (11; 18).

The main result of this chapter is now detailed here: The DNO is jointly analytic as a function of the parameters ε and δ, and the spatial variables x and y. Furthermore, the disk of analyticity can be centered at any (f_0, b_0), thereby including a neighborhood of the full, real two-plane in (ε, δ) space. In other words, setting $\eta(x) = f_0(x) + \varepsilon f(x)$ and $\zeta(x) = b_0(x) + \delta b(x)$, and given the velocity potential at the surface, $\xi(x)$, then both u and the DNO, can be written in the form of the Taylor expansions

$$u(x,y;\varepsilon,\delta) = \sum_{n=0}^{\infty}\sum_{m=0}^{\infty} u_{n,m}(x,y)\varepsilon^n\delta^m, \qquad G(x;\varepsilon,\delta)\xi = \sum_{n=0}^{\infty}\sum_{m=0}^{\infty} G_{n,m}(x)\xi\varepsilon^n\delta^m, \tag{3.43}$$

which converge strongly in the sense of the following two theorems.

Theorem 3.4.1. *If f, b, f_0, b_0 and ξ are real analyitic functions then*

$$\left\| \frac{\partial_x^k \partial_y^l}{(k+l)!} u_{n,m} \right\|_{H^2} \leq K_0 B^n D^m \frac{A^k}{(k+1)^2} \frac{E^l}{(l+1)^2}, \tag{3.44}$$

for constants K_0, B, D, A, $E > 0$.

Theorem 3.4.2. *If f, b, f_0, b_0 and ξ are real analyitic functions then*

$$\left\| \frac{\partial_x^k}{(k)!} G_{n,m} \xi \right\|_{H^2} \leq \tilde{K}_0 B^n D^m \frac{A^k}{(k+1)^2}, \tag{3.45}$$

for constants K_0, B, D, A, $E > 0$.

The proof of these general results is found in (23). The specific case of parametric analyticity in terms of simply ε and δ, i.e. $f_0 = b_0 = 0$ and when $(k, l) = (0, 0)$, will be stated with proof below.

Theorem 3.4.3. *Given $s \geq 0$, if f, $b \in C^{s+2}(P(\Gamma))$ and $\xi \in H^{s+3/2}(P(\Gamma))$, there exists a unique solution*

$$u(x, y; \varepsilon, \delta) = \sum_{n=0}^{\infty} \sum_{m=0}^{\infty} u_{n,m}(x, y) \varepsilon^n \delta^m$$

of Equation 3.35 satisfying

$$\|u_{n,m}\|_{H^{s+2}(P(\Gamma) \times [-h, 0])} \leq K_0 \|\xi\|_{H^{s+3/2}(P(\Gamma))} B^n D^m \tag{3.46}$$

for any $B > K(s, h, d)|f|_{C^{s+2}}$ and any $D > K(s, h, d)|b|_{C^{s+2}}$ and where K_0 is a universal constant. $K(s, h, d)$ will be defined in the following lemmas.

Theorem 3.4.4. *Given $s \geq 0$, if f, $b \in C^{s+2}(P(\Gamma))$ and $\xi \in H^{s+3/2}(P(\Gamma))$, then*

$$\|G_{n,m}\xi\|_{H^{s+1/2}(P(\Gamma))} \leq \tilde{K}_0 \|\xi\|_{H^{s+3/2}(P(\Gamma))} B^n D^m \tag{3.47}$$

for any $B > \tilde{K}(s,h,d)|f|_{C^{s+2}}$ and any $D > \tilde{K}(s,h,d)|b|_{C^{s+2}}$ and where $\tilde{K}_0$ is a universal constant. $\tilde{K}(s,h,d)$ will be defined in the following lemmas.

To prove these we need the following elliptic estimates (c.f. (11; 19)).

Lemma 3.4.5. *Given an integer $s \geq 0$, if $\xi \in H^{s+3/2}(P(\Gamma))$, $g^{(j)} \in H^{s+1}(P(\Gamma) \times [-h,0])$ and $\mathcal{J} \in H^{s+1/2}(P(\Gamma))$, then there exists a unique solution $w(x,y)$ of*

$$\Delta w(x,y) = div_x[g^{(1)}(x,y)] + \partial_y[g^{(2)}(x,y)] + g^{(3)}(x,y) \qquad \text{in } S_{h,0,0} \tag{3.48a}$$

$$w(x,0) = \xi(x), \tag{3.48b}$$

$$\partial_y w(x,-h) = \mathcal{J}(x), \tag{3.48c}$$

$$w(x+\gamma,y) = w(x,y) \qquad \text{for all } \gamma \in \Gamma \tag{3.48d}$$

satisfying

$$\|w\|_{H^{s+2}(P(\Gamma)\times[-h,0])} \leqslant K_0 \left[\|\xi\|_{H^{s+3/2}(P(\Gamma))} + \sum_{j=1}^{3} \|g^{(j)}\|_{H^{s+1}(P(\Gamma)\times[-h,0])} + \|\mathcal{J}\|_{H^{s+1/2}(P(\Gamma))} \right] \tag{3.49}$$

where K_0 is a universal constant.

Proof. This lemma is an extension of the periodic analogue of a theorem found in (12), where $\mathcal{J}(x) = 0$. Therefore, to prove this lemma, let $w(x,y) = w_1(x,y) + w_2(x,y)$, where $w_1(x,y)$

solves Equation 3.48 with $\mathcal{J}(x) = 0$ and $w_2(x,y)$ solves Equation 3.48 with $g^{(j)}\xi(x) = 0$. The theorem in (12) states that $w_1(x,y)$ must satisfy

$$\|w_1\|_{H^{s+2}(P(\Gamma)\times[-h,0])} \leq K_0 \left[\|\xi\|_{H^{s+3/2}(P(\Gamma))} + \sum_{j=1}^{3} \|g^{(j)}\|_{H^{s+1}(P(\Gamma))\times[-h,0]} \right]. \tag{3.50}$$

So then, to prove the lemma, all that is needed to still be shown is that $\|w_2\|_{H^{s+2}(P(\Gamma\times[-h,0]))} \leq K_0\|\mathcal{J}\|_{H^{s+1/2}(P(\Gamma))}$.

The spectral representation of $w_2(x,y)$ is given by

$$w_2(x,y) = \sum_{k\in\Gamma'} \frac{\sinh(|k|y)}{|k|\cosh(|k|h)} \hat{\mathcal{J}}(k) e^{ik\cdot x}. \tag{3.51}$$

Then

$$\begin{aligned}
\|w_2\|^2_{H^{s+2}(P(\Gamma)\times[-\mathrm{h},0])} &= \sum_{l=0}^{s}\sum_{k\in\Gamma'}\int_{-h}^{0} |\partial_y^l \hat{w}_2(k,y)|^2 dy \langle k\rangle^{2(s+2-l)} \\
&\leq \sum_{k\in\Gamma'}\sum_{l=0}^{s} \frac{|\hat{\mathcal{J}}(k)|^2 \sinh(2|k|h)\langle k\rangle^{2(s+2-l)}}{4|k|^3|k|^{-2l}\cosh^2(|k|h)} \\
&\leq \sum_{k\in\Gamma'}\sum_{l=0}^{s} \frac{|\hat{\mathcal{J}}(k)|^2 \sinh(2|k|h)\langle k\rangle^{2(s+2)}}{4|k|^3\cosh^2(|k|h)} \\
&\leq \sum_{k\in\Gamma'}\sum_{l=0}^{s} \frac{|\hat{\mathcal{J}}(k)|^2 \sinh(2|k|h)\langle k\rangle^{2(s+1/2)}}{2\cosh(2|k|h)} \\
&\leq \sum_{k\in\Gamma'}\sum_{l=0}^{s} |\hat{\mathcal{J}}(k)|^2 \langle k\rangle^{2(s+1/2)} \\
&\leq K_0\|\mathcal{J}\|^2_{H^{s+1/2}(P(\Gamma))}.
\end{aligned} \tag{3.52}$$

□

In light of Lemma 3.4.5, if one can obtain bounds on $F^{(i)}_{n,m}(x,y)$ $(i = 1,2,3)$ and $J_{n,m}(x)$, then we also have bounds on the functions $u_{n,m}$, proving Theorem 3.4.3. The proof of Theorem 3.4.3 and its corollary is, not surprisingly, inductive. While it would seem as though the induction would involve a double induction on both n and m, this need not be the case. From the formulas for the $F^{(i)}_{n,m}(x,y)$ $(i = 1,2,3)$ and $J_{n,m}(x)$, it is clear that they depend only on a finite number of precursors of $u_{n,m}$ of the form $u_{n-i,m-j}$ where $i + j \leq 2$. (So for any (n,m), $F^{(i)}_{n,m}(x,y)$ $(i = 1,2,3)$ and $J_{n,m}(x)$ depend on at most 5 precursors, namely $u_{n-1,m}$, $u_{n-2,m}$, $u_{n-1,m-1}$, $u_{n,m-1}$ and $u_{n,m-2}$). This allows us to perform a single induction on the, as yet, undefined index l.

Letting $n + m = l$, the induction will need to be started by not only showing the estimate holds in the $l = 0$ case, but that it holds in the $l = 1$ case as well. The case $l = 0$ $(m = n = 0)$, is a special case of Lemma 3.4.5 that $\|u_{0,0}\|_{H^{s+2}} \leq K_0\|\xi\|_{H^{s+3/2}(P(\Gamma))}$. The next two lemmas will show that the estimate in Equation 3.49 holds for the $l = 1$ case. The first for when $(m,n) = (1,0)$, and the second for when $(m,n) = (0,1)$.

Lemma 3.4.6. *Let $s \geq 0$ be an integer, $f \in C^{s+2}(P(\Gamma))$, and $B > K_1|f|_{C^{s+2}}$, where K_1 is some constant that depends only on h, s and d. Then*

$$\|u_{1,0}\|_{H^{s+2}(P(\Gamma)\times[-h,0])} \leqslant K_0\|\xi\|_{H^{s+3/2}(P(\Gamma))}B. \tag{3.53}$$

Proof. From Lemma 3.4.5 (note that $J_{1,0} = 0$),

$$\begin{aligned}
h\|u_{1,0}\|_{H^{s+2}(P(\Gamma)\times[-h,0])} &\leq K_0 \sum_{j=1}^{3} \|hF_{1,0}^{(j)}\|_{H^{s+1}(P(\Gamma)\times[-h,0])} \\
&\leq K_0\{\|2f\nabla_x u_{0,0}\|_{H^{s+1}(P(\Gamma)\times[-h,0])} \\
&\quad + \|(y+h)\nabla_x f \partial_y u_{0,0}\|_{H^{s+1}(P(\Gamma)\times[-h,0])} \\
&\quad + \|(y+h)\nabla_x f \cdot \nabla_x u_{0,0}\|_{H^{s+1}(P(\Gamma)\times[-h,0])} \\
&\quad + \|\nabla_x f \cdot \nabla_x u_{0,0}\|_{H^{s+1}(P(\Gamma])\times[-h,0])}\} \\
&\leq K_0\{2C(s+1)|f|_{C^{s+1}}\|\nabla_x u_{0,0}\|_{H^{s+1}(P(\Gamma)\times[-h,0])} \\
&\quad + C(s+1)|\nabla_x f|_{C^{s+1}}\|(y+h)\partial_y u_{0,0}\|_{H^{s+1}(P(\Gamma)\times[-h,0])} \\
&\quad + C(s+1)|\nabla_x f|_{C^{s+1}}\|(y+h)\nabla_x u_{0,0}\|_{H^{s+1}(P(\Gamma)\times[-h,0])} \\
&\quad + C(s+1)|\nabla_x f|_{C^{s+1}}\|\nabla_x u_{0,0}\|_{H^{s+1}(P(\Gamma)\times[-h,0])}\},
\end{aligned}$$

where we have used the fact that $\|fg\|_{H^s} \leqslant C(s)|f|_{C^s}\|g\|_{H^s}$. Continuing with the inequality,

$$h\|u_{1,0}\|_{H^{s+2}} \leq K_0 C\{3|f|_{C^{s+2}}\|u_{0,0}\|_{H^{s+2}} + 2Y|f|_{C^{s+2}}\|u_{0,0}\|_{H^{s+2}}\},$$

where Y is a constant such that $\|p_i(y)\nabla u\|_{H^s} \leq Y\|u\|_{H^{s+1}}$ for any $p_i(y) \in \{y, y+h, y^2, y(y+h), (y+h)^2\}$. Now we finish the inequality using the bounds on $u_{1,0}$ from Lemma 3.4.6,

$$\begin{aligned}
h\|u_{1,0}\|_{H^{s+2}} &\leq K_0 C(3+2Y)|f|_{C^{s+2}}\|u_{0,0}\|_{H^{s+2}} \\
&\leq hK_0K_1|f|_{C^{s+2}}\|\xi\|_{H^{s+3/2}}.
\end{aligned}$$

Here $K_1 = K_0 h^{-1}(3+2Y)C$. Then by choosing B large enough,

$$\|u_{1,0}\|_{H^{s+2}(P(\Gamma)\times[-\mathrm{h},0])} \leqslant K_0\|\xi\|_{H^{s+3/2}(P(\Gamma))}B.$$

□

Lemma 3.4.7. *Let $s \geq 0$ be an integer, $b \in C^{s+2}(P(\Gamma))$, and $D > K_2|b|_{C^{s+2}}$, where K_2 is some constant that depends only on h, s and d. Then*

$$\|u_{0,1}\|_{H^{s+2}(P(\Gamma)\times[-h,0])} \leq K_0\|\xi\|_{H^{s+3/2}(P(\Gamma))}D. \tag{3.54}$$

Proof. The proof is quite similar to the previous one, so we briefly sketch it here. Again starting from Lemma 3.4.5

$$
\begin{aligned}
h\|u_{0,1}\|_{H^{s+2}} &\le K_0 \left[\sum_{j=1}^{3} \|hF_{0,1}^{(j)}\|_{H^{s+1}} + \|hJ_{0,1}\|_{H^{s+1/2}} \right] \\
&\le K_0 \{ \|2b\nabla_x u_{0,0}\|_{H^{s+1}} + \|y\nabla_x b \partial_y u_{0,0}\|_{H^{s+1}} \\
&\quad + \|y\nabla_x b \cdot \nabla_x u_{0,0}\|_{H^{s+1}} + \|\nabla_x b \cdot \nabla_x u_{0,0}\|_{H^{s+1}} \\
&\quad + \|h\nabla_x b \cdot \nabla_x u_{0,0}(x,-h)\|_{H^{s+1/2}} \} \\
&\le K_0 \{ 2C(s+1)|b|_{C^{s+1}} \|\nabla_x u_{0,0}\|_{H^{s+1}} \\
&\quad + C(s+1)|\nabla_x b|_{C^{s+1}} \|y\partial_y u_{0,0}\|_{H^{s+1}} \\
&\quad + C(s+1)|\nabla_x b|_{C^{s+1}} \|y\nabla_x u_{0,0}\|_{H^{s+1}} \\
&\quad + C(s+1)|\nabla_x b|_{C^{s+1}} \|\nabla_x u_{0,0}\|_{H^{s+1}} \\
&\quad + hC(s+1/2)|\nabla_x b|_{C^{s+1/2+\alpha}} \|\nabla_x u_{0,0}\|_{H^{s+1/2}} \} \\
&\le K_0 C \{ 3|b|_{C^{s+2}} \|u_{0,0}\|_{H^{s+2}} \\
&\quad + 2Y|b|_{C^{s+2}} \|u_{0,0}\|_{H^{s+2}} \\
&\quad + h|b|_{C^{s+2}} \|u_{0,0}\|_{H^{s+2}} \} \\
&\le K_0 C(3+2Y+h)|b|_{C^{s+2}} K_0 \|\xi\|_{H^{s+3/2}} \\
&\le hK_0 K_2 |b|_{C^{s+2}} \|\xi\|_{H^{s+3/2}},
\end{aligned}
$$

where $K_2 = K_0 h^{-1}(3+2Y+h)C$; so given D sufficiently large,

$$
\|u_{0,1}\|_{C^{s+2}(P(\Gamma)\times[-\mathrm{h},0])} \quad \le \quad K_0 \|\xi\|_{H^{s+3/2}(P(\Gamma))} D.
$$

□

The next lemma uses the inductive hypothesis on l. As the full formulas for $F^{(j)}_{n,m}$ and $J_{n,m}$ quite lengthy, the only estimates that will be shown are those for $F^{(2)}_{n,m}$ and $J_{n,m}$. The other $F^{(j)}_{n,m}$ can be shown to be bounded in a similar manner.

Lemma 3.4.8. *Let $s \geq 0$ be an integer and let $b, f \in C^{s+2}(P(\Gamma))$. Assume*

$$\|u_{n,m}\|_{H^{s+2}(P(\Gamma)\times[-h,0])} \leq K_0 \|\xi\|_{H^{s+3/2}(P(\Gamma))} B^n D^m \tag{3.55}$$

for any (n,m) such that $n+m<L$. B and D are some constants. Then for any (N,M) such that $N+M=L$,

$$\|F^{(j)}_{N,M}\|_{H^{s+1}(P(\Gamma)\times[-h,0])} \leq K_0 \|\xi\|_{H^{s+3/2}(P(\Gamma))} K_{2+j} \sum_{i+k=1}^{2} |f|^i_{C^{s+2}} |b|^k_{C^{s+2}} B^{N-i} D^{M-k} \tag{3.56}$$

and

$$\|J_{N,M}\|_{H^{s+1/2}(P(\Gamma))} \leq K_0 \|\xi\|_{H^{s+3/2}(P(\Gamma))} K_6 \sum_{i+k=1}^{2} |f|^i_{C^{s+2}} |b|^k_{C^{s+2}} B^{N-i} D^{M-k} \tag{3.57}$$

where K_{2+j} $(j=1,2,3)$ and K_6 are constants that depend only on h, s and d.

Proof. As prevously stated, we will only show the estimates for $F^{(2)}_{N,M}$ and $J_{N,M}$. The other estimates are similar.

$$
\begin{aligned}
h^2\|F^{(2)}_{N,M}\|_{H^{s+1}} &\le h\|y\nabla_x b\cdot\nabla_x u_{N,M-1}\|_{H^{s+1}} + h\|(y+h)\nabla_x f\cdot\nabla_x u_{N-1,M}\|_{H^{s+1}}\\
&\quad + \|\frac{y}{2}\nabla_x(b^2)\cdot\nabla_x u_{N,M-2}\|_{H^{s+1}} + \|y^2|\nabla_x b|^2\partial_y u_{N,M-2}\|_{H^{s+1}}\\
&\quad + \|\frac{y+h}{2}\nabla_x(f^2)\cdot\nabla_x u_{N-2,M}\|_{H^{s+1}} + \|(y+h)^2|\nabla_x f|^2\partial_y u_{N-2,M}\|_{H^{s+1}}\\
&\quad + \|((y+h)b\nabla_x f - yf\nabla_x b)\cdot\nabla_x u_{N-1,M-1}\|_{H^{s+1}}\\
&\quad + \|2y(y+h)(\nabla_x f\cdot\nabla_x b)\partial_y u_{N-1,M-1}\|_{H^{s+1}}\\
&\le hC|\nabla_x b|_{C^{s+1}}\|y\nabla_x u_{N,M-1}\|_{H^{s+1}} + hC|\nabla_x f|_{C^{s+1}}\|(y+h)\nabla_x u_{N-1,M}\|_{H^{s+1}}\\
&\quad + C^2|\nabla_x b|_{C^{s+1}}|b|_{C^{s+1}}\|y\nabla_x u_{N,M-2}\|_{H^{s+1}} + C^2|\nabla_x b|^2_{C^{s+1}}\|y^2\partial_y u_{N,M-2}\|_{H^{s+1}}\\
&\quad + C^2|\nabla_x f|_{C^{s+1}}|f|_{C^{s+1}}\|(y+h)\nabla_x u_{N-2,M}\|_{H^{s+1}}\\
&\quad + C^2|\nabla_x f|^2_{C^{s+1}}\|(y+h)^2\partial_y u_{N-2,M}\|_{H^{s+1}}\\
&\quad + C^2|b|_{C^{s+1}}|\nabla_x f|_{C^{s+1}}\|(y+h)\nabla_x u_{N-1,M-1}\|_{H^{s+1}}\\
&\quad + C^2|f|_{C^{s+1}}|\nabla_x b|_{C^{s+1}}\|y\nabla_x u_{N-1,M-1}\|_{H^{s+1}}\\
&\quad + 2C^2|\nabla_x f|_{C^{s+1}}|\nabla_x b|_{C^{s+1}}\|y(y+h)\partial_y u_{N-1,M-1}\|_{H^{s+1}}\\
&\le hCY|b|_{C^{s+2}}\|u_{N,M-1}\|_{H^{s+2}} + hCY|f|_{C^{s+2}}\|u_{N-1,M}\|_{H^{s+2}}\\
&\quad + 2C^2Y|b|^2_{C^{s+2}}\|u_{N,M-2}\|_{H^{s+2}} + 2C^2Y|f|^2_{C^{s+2}}\|u_{N-2,M}\|_{H^{s+2}}\\
&\quad + 4C^2Y|f|_{C^{s+2}}|b|_{C^{s+2}}\|u_{N-1,M-1}\|_{H^{s+2}}\\
&\le K_0\|\xi\|_{H^{s+3/2}}\{hCY|b|_{C^{s+2}}B^N D^{M-1}\\
&\quad + hCY|f|_{C^{s+2}}B^{N-1}D^M + 2C^2Y|b|^2_{C^{s+2}}B^N D^{M-2}\\
&\quad + 2C^2Y|f|^2_{C^{s+2}}B^{N-2}D^M + 4C^2Y|f|_{C^{s+2}}|b|_{C^{s+2}}B^{N-1}D^{M-1}\}\\
&\le h^2K_0K_4\sum_{1\leqslant i+j\leqslant 2}|f|^i_{C^{s+2}}|b|^j_{C^{s+2}}B^{N-i}D^{M-j},
\end{aligned}
$$

where $K_4 = \max\{hCY, 4C^2Y\}$. Denoting $u = u(x, -h)$, we can likewise estimate:

$$\begin{aligned}
h\|J_{N,M}\|_{H^{s+1/2}} &\leq h\|\nabla_x b \cdot \nabla_x u_{N,M-1}\|_{H^{s+1/2}} \\
&\quad + \|b\nabla_x b \cdot \nabla_x u_{N,M-2}\|_{H^{s+1/2}} \\
&\quad + \|f\nabla_x b \cdot \nabla_x u_{N-1,M-1}\|_{H^{s+1/2}} \\
&\quad + h\|(|\nabla_x b|^2)\partial_y u_{N,M-2}\|_{H^{s+1/2}} \\
&\leq hC|\nabla_x b|_{C^{s+1/2+\alpha}}\|\nabla_x u_{N,M-1}\|_{H^{s+1/2}} \\
&\quad + C^2|b|_{C^{s+1/2+\alpha}}|\nabla_x b|_{C^{s+1/2}}\|\nabla_x u_{N,M-2}\|_{H^{s+1/2}} \\
&\quad + C^2|f|_{C^{s+1/2+\alpha}}|\nabla_x b|_{C^{s+1/2}}\|\nabla_x u_{N-1,M-1}\|_{H^{s+1/2}} \\
&\quad + hC^2|\nabla_x b|^2_{C^{s+1/2+\alpha}}\|\partial_y u_{N,M-2}\|_{H^{s+1/2}} \\
&\leq hC|b|_{C^{s+3/2}}\|u_{N,M-1}\|_{H^{s+3/2}} \\
&\quad + 2C^2|b|^2_{C^{s+3/2}}\|u_{N,M-1}\|_{H^{s+3/}} \\
&\quad + C^2|f|_{C^{s+3/2}}|b|_{C^{s+3/2}}\|u_{N-1,M-1}\|_{H^{s+3/2}} \\
&\leq K_0\|\xi\|_{H^{s+3/2}}\{hC|b|_{C^{s+3/2}}B^N D^{M-1} \\
&\quad + 2C^2|b|^2_{C^{s+3/2}}B^N D^{M-2} \\
&\quad + C^2|f|_{C^{s+3/2}}|b|_{C^{s+3/2}}B^{N-1}D^{M-1}\} \\
&\leq hK_0\|\xi\|_{H^{s+3/2}}K_6 \sum_{1\leqslant i+j\leqslant 2} |f|^i_{C^{s+2}}|b|^j_{C^{s+2}}B^{N-i}D^{M-j},
\end{aligned}$$

where $K_6 = \max\{C, 2h^{-1}C^2Y\}$. □

3.5 Proof of Analyticity

The proof of Theorem 3.4.3 is an induction on l where $l = n + m$.

Proof. The case when $l = 0$ follows directly from Lemma 3.4.5, as $g^{(j)}_{0,0} = 0$ and $\mathcal{J}(x) = 0$. The case for $l = 1$, i.e. $(m, n) = (1, 0)$ or $(m, n) = (0, 1)$, was shown in Lemmas 3.4.6 and 3.4.7.

Now assume that the estimate holds for all $l < L$, we now show that the estimate holds for $l = L$. From Lemma 3.4.5,

$$\begin{aligned}\|u_{N,M}\|_{H^{s+2}(P(\Gamma)\times[-h,0])} &\leqslant K_0 \left[\sum_{j=1}^{3} \|F^{(j)}_{N,M}\|_{H^{s+1}(P(\Gamma)\times[-h,0])} + \|J_{N,M}\|_{H^{s+1/2}(P(\Gamma))}\right] \\ &\leq K_0 K_0 \|\xi\|_{H^{s+3/2}(P(\Gamma))} \left[3K_7 \sum_{1\leqslant i+j\leqslant 2} |f|^i_{C^{s+2}} |b|^j_{C^{s+2}} B^{N-i} D^{M-j} \right. \\ &\quad \left. + K_6 \sum_{1\leqslant i+j\leqslant 2} |f|^i_{C^{s+2}} |b|^j_{C^{s+2}} B^{N-i} D^{M-j}\right].\end{aligned}$$

The second inequality follows from Lemma 3.4.8 with $K_7 = \max_{j=3,4,5}\{K_j\}$. Continuing with the inequality,

$$\|u_{N,M}\|_{H^{s+2}} \leq K_0 \|\xi\|_{H^{s+3/2}(P(\Gamma))} K_0(3K_7 + K_6) \sum_{1\leqslant i+j\leqslant 2} |f|^i_{C^{s+2}} |b|^j_{C^{s+2}} B^{N-i} D^{M-j},$$

so to obtain the desired estimate we must require that

$$K_0(3K_7 + K_6) \sum_{1\leqslant i+j\leqslant 2} |f|^i_{C^{s+2}} |b|^j_{C^{s+2}} B^{N-i} D^{M-j}. < B^N D^M$$

Choosing $K(h, s, d)$ as $K = \max\{K_0(3K_7 + K_6 h), [K_0(3K_7 + K_6 h)]^{1/2}, K_1, K_2\}$ and requiring that $B > \frac{K}{5}|f|_{C^{s+2}}$ and $D > \frac{K}{5}|b|_{C^{s+2}}$ we obtain

$$\|u_{N,M}\|_{H^{s+2}(P(\Gamma)\times[-h,0])} \leq K_0 \|\xi\|_{H^{s+3/2}(P(\Gamma))} B^N D^M.$$

□

We are now ready to prove the corollary of this result, Theorem 3.4.4, which establishes the analyticity of the DNO.

Proof. This is once again proven by induction on $l = n + m$. The case where $n + m = 0$ is trivial. $G_{0,0}(f, b)\xi = \partial_y u_{0,0}$, so

$$\begin{aligned}
\|G_{0,0}(f,b)\xi\|_{H^{s+1/2}(P(\Gamma))} &= \|\partial_y u_{0,0}\|_{H^{s+1/2}(P(\Gamma))} \\
&\leq \|u_{0,0}\|_{H^{s+2}(P(\Gamma))} \\
&\leq K_0\|\xi\|_{H^{s+3/2}(P(\Gamma))} \\
&\leq \frac{1}{6}\tilde{K}_0\|\xi\|_{H^{s+3/2}(P(\Gamma))} \\
&\leq \tilde{K}_0\|\xi\|_{H^{s+3/2}(P(\Gamma))}.
\end{aligned}$$

Above, we set $K_0 \leqslant (1/6)C_0$ for reasons that will be evident in the inductive step. Now assuming that the estimate holds for $l < L$, and checking the estimate for any (N, M) such that $N + M = L$:

$$
\begin{aligned}
\|G_{N,M}(f,b)\xi\|_{H^{s+1/2}} &\le \|\nabla_x f\cdot\nabla_x u_{N-1,M}\|_{H^{s+1/2}} \\
&\quad + h^{-1}\|b\nabla_x f\cdot\nabla_x u_{N-1,M-1}\|_{H^{s+1/2}} \\
&\quad + h^{-1}\|f\nabla_x f\cdot\nabla_x u_{N-2,M}\|_{H^{s+1/2}} \\
&\quad + \|\partial_y u_{N,M}\|_{H^{s+1/2}} + \|(|\nabla_x f|^2)\partial_y u_{N-2,M}\|_{H^{s+1/2}} \\
&\quad + \|fG_{N-1,M}(f,b)\xi\|_{H^{s+1/2}} + \|bG_{N,M-1}(f,b)\xi\|_{H^{s+1/2}} \\
&\le C|f|_{C^{s+2}}\|u_{N-1,M}\|_{H^{s+2}} + h^{-1}C^2|b|_{C^{s+2}}|f|_{C^{s+2}}\|u_{N-1,M-1}\|_{H^{s+2}} \\
&\quad + (1+h^{-1})C^2|f|^2_{C^{s+2}}\|u_{N-2,M}\|_{H^{s+2}} + \|\partial_y u_{N,M}\|_{H^{s+1/2}} \\
&\quad + C|f|_{C^{s+2}}\|G_{N-1,M}(f,b)\xi\|_{H^{s+1/2}} \\
&\quad + C|b|_{C^{s+2}}\|G_{N,M-1}(f,b)\xi\|_{H^{s+1/2}} \\
&\le K_0 C|f|_{C^{s+2}}\|\xi\|_{H^{s+3/2}}B^{N-1}D^M \\
&\quad + K_0 h^{-1}C^2|b|_{C^{s+2}}|f|_{C^{s+2}}\|\xi\|_{H^{s+3/2}}B^{N-1}D^{M-1} \\
&\quad + K_0(1+h^{-1})C^2|f|^2_{C^{s+2}}\|\xi\|_{H^{s+3/2}}B^{N-2}D^M \\
&\quad + K_0\|\xi\|_{H^{s+3/2}}B^N D^M \\
&\quad + \tilde{K}_0 C|f|_{C^{s+2}}\|\xi\|_{H^{s+3/2}}B^{N-1}D^M \\
&\quad + \tilde{K}_0 C|b|_{C^{s+2}}\|\xi\|_{H^{s+3/2}}B^N D^{M-1} \\
&\le \frac{1}{6}\tilde{K}_0\|\xi\|_{H^{s+3/2}}\{|f|_{C^{s+2}}B^{N-1}D^M \\
&\quad + h^{-1}C^2|b|_{C^{s+2}}|f|_{C^{s+2}}B^{N-1}D^{M-1} \\
&\quad + (1+h^{-1})C^2|f|^2_{C^{s+2}}B^{N-2}D^M \\
&\quad + B^N D^M + 6C|f|_{C^{s+2}}B^{N-1}D^M \\
&\quad + 6C|b|_{C^{s+2}}B^N D^{M-1}\} \\
&\le \tilde{K}_0\|\xi\|_{H^{s+3/2}}B^N D^M.
\end{aligned}
$$

The last line is assured if we choose $\tilde{K}$ is defined as $\tilde{K} = \max\{1, \sqrt{1+h^{-1}}C, 6C\}$. $\square$

CHAPTER 4

A NON-TRADITIONAL INVERSE METHOD FOR DETERMINING BOTTOM TOPOGRAPHY

The DNO's usefulness extends past its application to the classical problem of water waves, or other classical PDE problems. It has also found a usefulness in solving certain inverse problems. The goal for this chapter is to define a specific inverse problem, the motivation of which is to determine ocean bathometry from surface measurements. This is quite different than the standard underwater acoustical method not only because it uses a fluid mechanics perspective, but also because the method is fundamentally nonlinear. Using the expansion of the DNO, and making an ansatz of standing-wave input data, methods of order one, two, and $M \geq 3$ will be developed and tested.

4.1 A General Method

For ease of reference, the governing equations are listed again:

$$\Delta\varphi = 0 \qquad \text{in } S_{h,\zeta,\eta} \tag{4.1a}$$

$$\partial_t\eta - \partial_y\varphi + \nabla_x\eta \cdot \nabla_x\varphi = 0 \qquad \text{on } y = \eta(x,t) \tag{4.1b}$$

$$\partial_t\varphi + g\eta + \frac{1}{2}|\nabla\varphi|^2 = 0 \qquad \text{on } y = \eta(x,t) \tag{4.1c}$$

$$\partial_y\varphi - \nabla_x\zeta \cdot \nabla_x\varphi = 0 \qquad \text{on } y = -h + \zeta(x). \tag{4.1d}$$

The definition of the DNO came as a necessity of reformulating Equation 4.1 on the upper boundary in terms of the surface variables $\eta(x,t)$ and $\xi(x,t) = \varphi(x,\eta(x,t),t)$. Ironically, it

is this upper surface reformulation that forms the basis of a method for finding the bottom contour given surface data. In Chapter 2 it was shown that Equation 4.1 could be reformulated on the surface as a Hamiltonian system with canonical variables ξ and η. This reformulation, however, is implicit in nature, and so we develop a more convenient and explicit one.

Recall the two boundary conditions at the surface $y = \eta$, the kinematic condition $\partial_t \eta + \nabla_x \varphi \cdot \nabla_x \eta - \partial_y \varphi = 0$ and Bernoulli's equation $\partial_t \varphi + \frac{1}{2}|\nabla \varphi|^2 + g\eta = 0$. These conditions are not explicitly written in terms of the canonical variables ξ and η from Zakharov's Hamiltonian system. For instance, Bernoulli's equation needs to be rewritten in terms of $\partial_t \xi$ and $\nabla_x \xi$ instead of $\partial_t \varphi$ and $\nabla \varphi$. Also, the kinematic condition includes a term with φ, but upon solving for $\partial_t \eta$, it is obvious that $\partial_t \varphi$ is equal to the definition of the DNO. Therefore,

$$\partial_t \eta(x,t) = G(\eta, \zeta)\xi(x,t). \tag{4.2}$$

Note that Equation 4.2 is now written explicitly in terms of ξ and η. To write the Bernoulli equation in terms of $\partial_t \xi$, the chain rule is applied to the definition of ξ. Recall the definition of $\xi(x)$,

$$\xi(x,t) = \varphi(x, \eta(x,t), t). \tag{4.3}$$

The chain rule then implies that

$$\partial_t \varphi(x, \eta(x,t), t) = \partial_t \xi(x,t) - \partial_y \varphi(x, \eta(x,t), t)\partial_t \eta(x,t). \tag{4.4}$$

Substituting this expression into Bernoulli's equation and solving for $\partial_t \xi$ results in

$$\partial_t \xi(x,t) = -\frac{1}{2}|\nabla\varphi(x,\eta(x,t),t)|^2 - g\eta(x,t) + \partial_y\varphi(x,\eta(x,t),t)\partial_t\eta(x,t). \tag{4.5}$$

So all that needs to be done to write Equation 4.5 in terms of the canonical variables ξ and η is to have a set of explicit equations for $\nabla_x\varphi$ and $\partial_y\varphi$ in terms of ξ and η. To this end, we apply ∇_x to both sides of Equation 4.3, and recall the definition of the DNO:

$$\nabla_x\xi = \nabla_x\varphi + \partial_y\varphi\nabla_x\eta \tag{4.6a}$$

$$G(\eta,\zeta)\xi = -\nabla_x\eta\cdot\nabla_x\varphi + \partial_y\varphi. \tag{4.6b}$$

This system of equations can be viewed as a system of two equations with two unknowns–$\nabla_x\varphi$ and $\partial_y\varphi$–which can then be solved using basic linear algebra. To accomplish this we first take the dot product of Equation 4.6a with $\nabla_x\eta$, and add the result to Equation 4.6b, which gives

$$\partial_y\varphi = \frac{1}{\tilde{N}}\Big[\nabla_x\eta\cdot\nabla_x\xi + G(\eta,\zeta)\xi\Big], \tag{4.7}$$

where $\tilde{N} = 1 + |\nabla_x\eta|^2$. Upon insertion of this expression into Equation 4.6a, $\nabla_x\varphi$ takes the form

$$\nabla_x\varphi = \nabla_x\xi - \frac{G(\eta,\zeta)\xi + \nabla_x\eta\cdot\nabla_x\zeta}{\tilde{N}}\nabla_x\eta. \tag{4.8}$$

As there are now explicit formulas for $\nabla_x\varphi$ and $\partial_y\varphi$, they can be substituted into Equation 4.6a, and the explicit evolution equations for η and ξ are complete (10):

$$\partial_t\eta = G(\eta,\zeta)\xi \tag{4.9a}$$

$$\begin{aligned}\partial_t\xi = -g\eta - \frac{1}{2(1+|\nabla_x\eta|^2)}\Big[&|\nabla_x\xi|^2 - (G(\eta,\zeta)\xi)^2 \\ &-2[G(\eta,\zeta)\xi]\nabla_x\eta\cdot\nabla_x\xi + |\nabla_x\xi|^2|\nabla_x\eta|^2 - (\nabla_x\xi\cdot\nabla_x\eta)^2\Big].\end{aligned} \tag{4.9b}$$

We now consider small deviations from the quiescent state ($\eta_0 = 0, \xi_0 = 0$) and suppose that $\xi(x,t) = \varepsilon\tilde{\xi}(x,t)$ and $\eta(x,t) = \varepsilon\tilde{\eta}(x,t)$.

Remark 4.1.1. *This ε is not intended to be the same parameter used in the previous chapter, but is used purely to emphasize the small deviation from a flat surface. Also, from this point forward let $d = 2$ for computational and notational purposes. As such, ∇_x will be replaced by ∂_x.*

In theory, given full information about $\eta(x,t)$ and $\xi(x,t)$, one should be able to use Equation 4.9 to determine $\zeta(x)$. Even when the quadratic terms in Equation 4.9b are ignored, this task is clearly unattractive as the expansion for the DNO, as seen in earlier chapters, is quite involved. To simplify, keeping only terms of up to $O(\varepsilon)$, the system comprised of Equation 4.9a and Equation 4.9b becomes:

$$\partial_t\tilde{\xi} = -g\tilde{\eta}, \qquad \partial_t\tilde{\eta} = G(0,\zeta)\tilde{\xi}. \tag{4.10}$$

To make the notation less cumbersome, the tildes will be dropped. Taking a time derivative on the second equation and substituting the first into the second results in a single equation for η,

$$\partial_t^2 \eta = -gG(0,\zeta)\eta, \tag{4.11}$$

which forms the basis of the proposed inverse method.

Notice that while the surface quantities have been linearized, at this point the DNO retains its full nonlinear dependance on ζ. Also, while the DNO has, up to this point, acted solely on the Dirichlet data ξ, it is now viewed formally as an operator that acts on the surface deformation η. Equation 4.11 expresses the inverse problem, which is: given surface measurements of η, find ζ. The difficulty in this problem lies in the fact that the DNO depends on ζ in a truly nonlinear way.

4.2 A Partial Expansion of the DNO–Operator Expansion

In the previous chapter, the DNO was expanded into a double perturbation series, where the geometry of our system was viewed as a perturbation of the system with flat bottom and top boundaries. In a slight change in theme, we see from Equation 4.11 that we may few the top deformation as negligible. When $\eta(x) = 0$ and $\zeta(x)$ is arbitrary, the solution to Equation 2.8 is given by

$$\varphi(x,y) = \frac{\cosh((y+h)D)}{\cosh(hD)}\xi(x) + \sinh(yD)(L(\zeta)\xi)(x), \tag{4.12}$$

where $L(\zeta)$ is an implicit operator that acts on $\xi(x)$ (see (7) . Then inserting Equation 4.12 into the definition of the DNO results in

$$G(0,\zeta)\xi = \partial_y\varphi|_{y=0} = D\tanh(hD)\xi + D(L(\zeta)\xi), \tag{4.13}$$

and we expand the DNO in terms of the bottom perturbation, $\zeta = \delta b$, alone

$$G(0,\zeta)\xi = \sum_{m=0}^{\infty} G_m(0,b)[\xi]\delta^m. \tag{4.14}$$

Remark 4.2.1. *Note that the $G_m(0,b)$ corresponds to the $G_{0,m}$ from the double series expansion in the previous chapter. But since there won't be a double sum, the extra index is dropped to simplify the notation. Also, as there is no η dependance, we define $G_m(b) = G_m(0,b)$.*

In light of Equation 4.13 and Equation 4.14, the DNO can now be written as

$$\begin{aligned} G(\zeta)\xi &= G_0(b)\xi + \sum_{m=1}^{\infty}(G_m(b)\xi)\delta^m \\ &= D\tanh(hD)\xi + \sum_{m=1}^{\infty}(G_m(b)\xi)\delta^m. \end{aligned} \tag{4.15}$$

It becomes evident from Equation 4.13 and Equation 4.15, that expanding the DNO is equivalent to finding an expansion for the operator L. In other words, by expanding L,

$$L(\delta b)\xi = \sum_{m=1}^{\infty} L_m(b)[\xi]\delta^m \tag{4.16}$$

it is easy to see (comparing Equation 4.15 to Equation 4.13) that for $m > 0$

$$G_m(b)\xi = DL_m(b)\xi. \tag{4.17}$$

To demonstrate the "Operator Expansion" approach, it will be used to expand $L(\zeta)$ in a perturbation series. This method was used in (7) to expand the DNO in a double perturbation series (for the case when $\eta \neq 0$). Since there is a solution (Equation 4.12) of the system Equation 2.8 when $\eta(x) = 0$, it can be substituted into the Neumann condition on the bottom boundary:

$$\partial_y\varphi - \partial_x\varphi\partial_x\zeta = 0 \qquad \text{at } y = -h + \zeta(x),$$

in preparation to expand the operator around $y = -h$. The Neumann condition takes the form

$$\left[D\frac{\sinh(\zeta D)}{\cosh(hD)} + D\cosh((\zeta - h)D)L(\zeta)\right]\xi + (D\zeta)\left[\frac{\cosh(\zeta D)}{\cosh(hD)} + \sinh((\zeta - h)D)L(\zeta)\right]D\xi = 0. \tag{4.18}$$

The various hyperbolic trigonometric functions can be expanded in Taylor series which will be included here for ease of reference.

$$\sinh(\zeta D) = \sum_{\substack{j=1 \\ \text{odd}}}^{\infty} \frac{(\zeta D)^j}{j!}, \qquad \cosh(\zeta D) = \sum_{\substack{j=0 \\ \text{even}}}^{\infty} \frac{(\zeta D)^j}{j!}.$$

For the other functions, the sum/difference formulas for trigonometric functions will be applied previous to the expansions:

$$\begin{aligned}
\cosh(\zeta D - hD) &= \cosh(\zeta D)\cosh(hD) - \sinh(\zeta D)\sinh(hD) \\
&= \sum_{\substack{j=0 \\ \text{even}}}^{\infty} \frac{(\zeta D)^j}{j!}\cosh(hD) - \sum_{\substack{j=1 \\ \text{odd}}}^{\infty} \frac{(\zeta D)^j}{j!}\sinh(hD) \\
\sinh(\zeta D - hD) &= \sinh(\zeta D)\cosh(hD) - \cosh(\zeta D)\sinh(hD) \\
&= \sum_{\substack{j=1 \\ \text{odd}}}^{\infty} \frac{(\zeta D)^j}{j!}\cosh(hD) - \sum_{\substack{j=0 \\ \text{even}}}^{\infty} \frac{(\zeta D)^j}{j!}\sinh(hD).
\end{aligned}$$

These expansions can be substituted into Equation 4.18:

$$\begin{aligned}
0 = \sum_{\substack{j=1 \\ \text{odd}}}^{\infty} \left[(D\zeta)\frac{\zeta^j}{j!}\cosh(hD)D^jL(\zeta) + D\frac{\zeta^j}{j!}(\operatorname{sech}(hD)D^j - \sinh(hD)D^jL(\zeta)) \right] + \\
\sum_{\substack{j=0 \\ \text{even}}}^{\infty} \left[D\frac{\zeta^j}{j!}\cosh(hD)D^jL(\zeta) + (D\zeta)\frac{\zeta^j}{j!}(\operatorname{sech}(hD)D^j - \sinh(hD)D^jL(\zeta)) \right]. \quad (4.19)
\end{aligned}$$

In the spirit of earlier chapters, the bottom boundary is now viewed as a small perturbation of the trivial bottom boundary. Letting $\zeta(x) = \delta b(x)$ and inserting Equation 4.16 into Equa-

tion 4.19, the various $L_m(b)$ can be identified by collecting terms of the same order of δ. Then for m odd:

$$L_m(b) = -\text{sech}(hD)\left(\sum_{\substack{j=2\\ \text{even}}}^{m-1}\left[\frac{b^j}{j!}\cosh(hD)D^jL_{m-j}(b)\right] - \sum_{\substack{j=1\\ \text{odd}}}^{m-2}\left[\frac{b^j}{j!}\sinh(hD)D^jL_{m-j}(b)\right] + \frac{b^m}{m!}\text{sech}(hD)D^m\right), \quad (4.20)$$

and for m even:

$$L_m(b) = -\text{sech}(hD)\left(\sum_{\substack{j=2\\ \text{even}}}^{m-2}\left[\frac{b^j}{j!}\cosh(hD)D^jL_{m-j}(b)\right] - \sum_{\substack{j=1\\ \text{odd}}}^{m-1}\left[\frac{b^j}{j!}\sinh(hD)D^jL_{m-j}(b)\right]\right). \quad (4.21)$$

From the above formulas, one can calculate the first few terms of the expansion which will become quite important in the next section. For instance:

$$L_1(b) = -\text{sech}(hD)b\text{sech}(hD)D, \qquad L_2(b) = \text{sech}(hD)b\sinh(hD)DL_1(b). \quad (4.22)$$

From Equation 4.22, we see that the calculation of $G_{0,1} = G_1$ from the "Field Expansions" section is confirmed, and $G_{0,2} = G_2$ is also calculated for good measure:

$$G_1(b) = -D\text{sech}(hD)b\text{sech}(hD)D, \qquad G_2(b) = D\text{sech}(hD)b\sinh(hD)G_1(b). \quad (4.23)$$

As is evident from the above formulas, the pseudo-differential operator $D\text{sech}(hD)$ makes repeated occurences in the DNO's expansion, so let $\tilde{D} = D\text{sech}(hD)$. Note that now G_2 takes on the quite simple form:

$$G_2 = -\tilde{D}bG_0b\tilde{D}; \tag{4.24}$$

the convenience of this compact form becomes evident when second and higher order methods based on factoring are discussed.

4.3 Craig's First Order Formula

Now that the DNO is partially expanded, a first order inverse method by Craig (6) can be devised. Returning to the general inverse method,

$$\partial_t^2\eta = -gG(\zeta)\eta, \tag{4.25}$$

one last assumption is made–the assumption that the wave forms are standing waves, i.e. $\eta(x,t) = \bar{\eta}(x)e^{i\omega t}$ with frequency ω and envelope $\bar{\eta}(x)$. When this expression is substituted into Equation 4.25 and simplified, the expression becomes a basic eigenvalue problem:

$$\frac{\omega^2}{g}\bar{\eta}(x) = G(\zeta)\bar{\eta}(x) = D\tanh(hD)\bar{\eta}(x) + \sum_{m=1}^{\infty} G_m(b)\bar{\eta}(x)\delta^m \tag{4.26}$$

Now truncating the expansion of the DNO at $O(\delta^2)$, a first order equation is constructed:

$$\frac{\omega^2}{g}\bar{\eta}(x) = \left[G_0(b) + G_1(b)\right]\bar{\eta}(x). \tag{4.27}$$

Substituting the formulas for G_0 and G_1 into the above equation, and putting the term with $b(x)$ to one side, and all other terms to the other side results in:

$$\tilde{D}b(x)\tilde{D}\bar{\eta}(x) = \left(G_0 - \frac{\omega^2}{g}\right)\bar{\eta}(x). \tag{4.28}$$

This expression can be formally solved for $b(x)$, which then gives the formula of Craig (6)

$$b(x) = \frac{\left[\sinh(hD) - (\omega^2/g)D^{-1}\cosh(hD)\right]\bar{\eta}(x)}{\tilde{D}\bar{\eta}(x)}. \tag{4.29}$$

This expression, however, creates multiple problems. In the numerator, $D^{-1}\cosh(hD)$ is an operator that amplifies large wave numbers. In the denominator, whenever $\tilde{D}\bar{\eta}(x) = 0$ the expression is undefined. Backing up a step to see how to circumvent these problems, both sides of Equation 4.28 are multiplied by $\tilde{D}^{-1} = D^{-1}\cosh(hD)$, to give

$$b(x)\left[\tilde{D}\bar{\eta}(x)\right] = \left[\sinh(hD) - (\omega^2/g)\tilde{D}^{-1}\right]\bar{\eta}(x). \tag{4.30}$$

We now define the following functions:

$$l^{(0)}(x) = \tilde{D}\bar{\eta}(x), \qquad r^{(0)}(x) = \left[\sinh(hD) - (\omega^2/g)\tilde{D}^{-1}\right]\bar{\eta}(x). \tag{4.31}$$

This results in the very simple equation $b(x)l^{(0)}(x) = r^{(0)}(x)$. Recall that one of the problems with Equation 4.29 is that it might be undefined at certain values of x where the denominator is zero. It certainly would be agreeable to the situation if the bottom $b(x)$ is assumed to be continuous. If differentiability is assumed in addition to the continuity of $l^{(0)}(x), b(x)$ and

$r^{(0)}(x)$, a derivative can be taken on $b(x)l^{(0)}(x) = r^{(0)}(x)$, which defines an operator that depends on $l^{(0)}(x)$ and acts on $b(x)$.

$$A_l b(x) = \partial_x r^{(0)}(x) \tag{4.32}$$

where $A_l = \partial_x l^{(0)}(x) + l^{(0)}(x)\partial_x$. Not surprisingly this operator is singular, but using a singular-value decomposition spectral cut-off method (see Appendix A), a pseudo-inverse can be found to get an approximate solution to $b(x)$. The second problem of higher wave numbers being amplified through the operator $D^{-1}\cosh(hD)$ can be resolved using one of many filtering schemes. In the numerical testing of this and higher order methods, we utilize a low-pass filter which leaves low wavenumbers alone while setting high wavenumbers to zero.

4.4 A Few Second Order Algorithms

Several second order algorithms can arise from Equation 4.11. It is here that the highly nonlinear nature of the DNO really starts to create some problems. Unlike in the Craig formula, $b(x)$ can not be easily identified in higher order methods. To get around this problem, an iterative approach must be taken, which uses the Craig formula as an initial seed value for the algorithm. While there is the obvious second order method of adding $G_2(b)$ to the right side of Equation 4.27 and using a Picard iteration, there are multiple ways to factor the operator $G_1 + G_2$ which lead to slightly different recursive equations, some of which result in formulas with better behaved operators.

4.4.1 Picard Iteration

A natural attempt for a second order algorithm would be to add the second order term to the right hand side of Equation 4.27

$$\omega^2\bar{\eta}(x) = g\left[G_0(b) + G_1(b) + G_2(b)\right]\bar{\eta}(x). \tag{4.33}$$

The terms can be rearranged so that the equation is in a similar form to Equation 4.28

$$\tilde{D}b(x)\tilde{D}\bar{\eta}(x) = \left(G_0 - \frac{\omega^2}{g}\right)\bar{\eta}(x) + G_2(b)\bar{\eta}(x). \tag{4.34}$$

Craig's formula Equation 4.29 is used to find $b_0(x)$, and the following iteration is set up:

$$\tilde{D}b_j(x)\tilde{D}\bar{\eta}(x) = \left(G_0 - \frac{\omega^2}{g}\right)\bar{\eta}(x) + G_2(b_{j-1})\bar{\eta}(x). \tag{4.35}$$

This iteration is then solved using the same methods developed for Craig's formula. That is, it is simplified first by multiplying both sides by $\tilde{D}^{-1}$ resulting in

$$b_j\tilde{D}\bar{\eta} = \left(\sinh(hD) - \frac{\omega^2}{g}\tilde{D}^{-1}\right)\bar{\eta} - b_{j-1}G_0b_{j-1}\tilde{D}\bar{\eta}. \tag{4.36}$$

The equation now has a similar form to that seen in Equation 4.30. Indeed Equation 4.36 takes the form

$$b_j(x)l^{(0)}(x) = r_j^{(1)}(x), \tag{4.37}$$

where $r_0^{(1)}(x) = r^{(0)}(x)$, and for $j \neq 0$,

$$r_j^{(1)}(x) = \left[\sinh(hD) - (\omega^2/g)\tilde{D}^{-1}\right]\bar{\eta}(x) - b_{j-1}(x)G_0(b_{j-1})\bar{\eta}(x). \tag{4.38}$$

So at $j = 0$, Equation 4.37 is Craig's formula which gives b_0. Once b_0 is found, the successive b_j's can be found using the same spectral cut-off/filtering method used in Craig's formula. This second order Picard method will be referred to as "2P".

4.4.2 Second Order Methods Derived From Factoring

There are two other second order algorithms based on Equation 4.11 that will be discussed. These two other methods are based on factoring $G_1 + G_2$. How this factoring helps find $b(x)$ becomes more obvious when Equation 4.33 is slightly rearranged into

$$[G_1(b) + G_2(b)]\,\bar{\eta}(x) = \left(G_0 - (\omega^2/g)\right)\bar{\eta}(x). \tag{4.39}$$

The left hand side of Equation 4.39 can be factored to the right and to the left:

$$\begin{aligned} G_1(b) + G_2(b) &= -\tilde{D}b(x)\tilde{D} - \tilde{D}b(x)G_0b(x)\tilde{D} \\ &= -\tilde{D}\left[b(x) + b(x)G_0b(x)\right]\tilde{D}. \end{aligned} \tag{4.40}$$

At this point, a choice can be made in how to further factor $G_1 + G_2$. This choice leads to what will be denoted the "Second Order, Right Factorization" $[b + bG_0b] = [I + bG_0]b$, and the "Second Order, Left Factorization" $[b + bG_0b] = b[I + G_0b]$, which will be referred to as "2R" and "2L" respectively.

Factoring $b(x)$ to the right in order to derive 2R results in the recursion

$$b_j(x)l^{(0)}(x) = r_j^{(2)}(x), \tag{4.41}$$

where $r_0^{(2)}(x) = r^{(0)}(x)$, and for $j \neq 0$

$$r_j^{(2)}(x) = [I + b_{j-1}(x)G_0]^{-1} r^{(0)}(x). \tag{4.42}$$

Factoring $b(x)$ to the left in order to derive 2L results in the recursion

$$b_j(x)l_j^{(1)}(x) = r^{(0)}(x), \tag{4.43}$$

where $l_0^{(1)}(x) = l^{(0)}(x)$, and for $j \neq 0$

$$l_j^{(1)}(x) = [I + G_0 b_{j-1}(x)]\, l^{(0)}(x). \tag{4.44}$$

4.5 Higher Order Methods

Of course, higher order methods can be developed in the same spirit as the second order methods. Naturally, an M^{th} order Picard method can be set up. Also, the existence of the second order methods derived from factoring $G_1 + G_2$, suggests that a similar factoring might be possible for $G_1 + G_2 + \cdots + G_m$. Indeed, it is possible to factor the DNO in a similar fashion as 2L, but it is not possible to factor in the same way as 2R. The reason for not being able to "factor to the right" has to do with the "extra" term $\frac{b^m}{m!}\text{sech}(hD)D^m$ in L_m with m odd.

The higher order methods are easier to develop if a factored form of the DNO expansion is used. Noting again that $G_m = DL_m$, it is evident from Equation 4.20 and Equation 4.21 that $\tilde{D}b(x)$ is on the left of every term in the expansion of G_m, and also, through simple inductive reasoning, that $\tilde{D}$ is on the right of every term in G_m. Therefore, it is possible to write each term of the DNO expansion G_m $(m \geq 1)$ in the form

$$G_m(b) = \tilde{D}b\tilde{G}_m(b)\tilde{D}. \tag{4.45}$$

Using this form for the DNO and the fact that $G_m = DL_m$ in Equation 4.20 and Equation 4.21 results in, for m odd,

$$\tilde{G}_m(b) = \sum_{\substack{j=1 \\ \text{odd}}}^{m-2} \left[\frac{b^{j-1}}{j!} \tanh(hD) D^j b(x) \tilde{G}_{m-j}(b) \right] - \sum_{\substack{j=2 \\ \text{even}}}^{m-1} \left[\frac{b^{j-1}}{j!} D^j b(x) \tilde{G}_{m-j}(b) \right] + \frac{b^{n-1}}{n!} D^{n-1}, \tag{4.46a}$$

and for m even,

$$\tilde{G}_m(b) = \sum_{\substack{j=1 \\ \text{odd}}}^{m-1} \left[\frac{b^{j-1}}{j!} \tanh(hD) D^j b \tilde{G}_{m-j}(b) \right] - \sum_{\substack{j=2 \\ \text{even}}}^{m-2} \left[\frac{b^{j-1}}{j!} D^j b(x) \tilde{G}_{m-j}(b) \right]. \tag{4.46b}$$

It is also interesting to note that there is now an absence of the ill-conditioned operators $\cosh(hD)$ and $\sinh(hD)$.

4.5.1 M^{th} Order Picard

Of course, an M^{th} order Picard iteration can also be set up. Extending the idea from Equation 4.35,

$$\tilde{D}b_j(x)\tilde{D}\bar{\eta}(x) = \left(G_0 - \frac{\omega^2}{g}\right)\bar{\eta}(x) - \tilde{D}b_{j-1}(x)\sum_{m=2}^{M}\tilde{G}_m(b_{j-1})\tilde{D}\bar{\eta}(x). \tag{4.47}$$

After applying $\tilde{D}^{-1}$ to both sides, we set up the recursion:

$$b_j(x)l^{(0)}(x) = r_j^{(3)}(x), \tag{4.48}$$

where $r_0^{(3)}(x) = r^{(0)}(x)$, and for $j \neq 0$,

$$r_j^{(3)}(x) = r^{(0)}(x) - \tilde{D}b_{j-1}(x)\sum_{m=2}^{M}\tilde{G}_m(b_{j-1})\tilde{D}\bar{\eta}(x). \tag{4.49}$$

This method will be referred to as "MP".

4.5.2 M^{th} Order Left Factorization

From the factorization Equation 4.46 an M^{th} order method can be developed which will be referred to as "ML". First, an M^{th} order generalization of Equation 4.39 is made.

$$\sum_{m=1}^{M}G_m(b)\bar{\eta}(x) = \left(G_0 - (\omega^2/g)\right)\bar{\eta}(x). \tag{4.50}$$

From Equation 4.45, the left-hand side of the above equation can be written as

$$\tilde{D}b(x)\left[\sum_{m=1}^{M}\tilde{G}_m(b)\right]\tilde{D}\bar{\eta}(x) = \left(G_0 - (\omega^2/g)\right)\bar{\eta}(x). \tag{4.51}$$

After multiplying both sides of the above equation by $\tilde{D}^{-1}$, we see the familiar recursion

$$b_j(x)l_j^{(2)}(x) = r^{(0)}(x), \tag{4.52}$$

where $l_0^{(2)}(x) = l^{(0)}(x)$, and for $j \neq 0$

$$l_j^{(2)}(x) = \sum_{m=1}^{M}\tilde{G}_m(b_{j-1})l^{(0)}(x). \tag{4.53}$$

As in the second order methods. Once b_0 is identified using Craig's formula, the successive b_j's are found using the spectral cut-off/filtering methods used in Craig's formula.

CHAPTER 5

NUMERICAL RESULTS

As the inverse methods proposed in the previous chapter are highly ill-conditioned, numerical validation of these methods is necessary not only to confirm their validity, but also to explore what types of bottom contours can be recovered. This chapter will detail the numerical tests that the various methods will undergo. The general method for testing involves inputting a given bottom contour into the forward problem Equation 4.26 to find a wave/frequency pair $(\overline{\eta}, \omega)$, and then use this data in the algorithms to reconstruct the original input.

5.1 Method for Numerical Testing

To test our results, we chose various representative bottom contours, solved the forward eigenvalue problem $\sum G_m(b)\eta(x) = (\omega^2/g)\eta(x)$ (from this point forward $g = 1$), and then chose one of the resulting eigenfunctions, eigenvalue pairs (η, ω) of lower frequency ω to represent a wave we would expect to find in the physical world. We then took that eigenfunction, and used it as the initial data for the inverse methods. The two representative contour families that will be tested tested are of the form

$$\zeta_1(x) = a\text{sech}(bx), \qquad 0 < a \lesssim h/2, \quad .5 \lesssim b \lesssim 8 \quad \text{and} \quad .25 \lesssim h \lesssim .85 \quad \text{(5.1a)}$$

$$\zeta_2(x) = a[\tanh(b(x+c)) - \tanh(b(x-c))],$$

$$0 < a \lesssim h/4, \quad .5 \lesssim b \lesssim 8, \quad \pi/4 \lesssim c \lesssim 4\pi/5 \quad \text{and} \quad .25 \lesssim h \lesssim .85. \quad (5.1b)$$

The purpose for these choices is so that ζ_1 might represent a typical single deviation of the bottom, like a Gaussian, and ζ_2 might represent a typical small symmetrical sandbar.

The methods that will be tested are all of the second order methods (2P, 2L and 2R), together with the fifth order Picard method "5P", and the fifth order, left factored method "5L". The testing will be divided up into six groups. The first group will show that the method does, in fact, work. Figures from these test will show the rate of convergence as a method and convergence to the original input. The second group will give two representative examples comparing the first (Craig's formula), second and fifth order approximations against the original bottom contour. The third and fourth groups graph the errors of the second and fifth order approximations respectively as the parameters from each family of functions $\zeta^{(1)}$ and $\zeta^{(2)}$ are varied. The fifth group will show how well the methods perform when noise is added to the input of the inverse methods. The noise will be added to $\overline{\eta}$ as well as to the frequency ω. The sixth group will show some approximations to a few other representative bottom contours in order to test the proposed algorithms in other situations that might be of interest. The error in each graph represents the L^∞ error.

Remark 5.1.1. *These parameter values will be used throughout the numerical testing. The only exception is when individual parameters are varied. The other parameters will be held constant at the above values.*

5.2 Convergence

Figure 1a, Figure 2a and Figure 3a display the convergence properties of the various methods for $\zeta^{(1)}$, while Figure 1b, Figure 2b and Figure 3b display the convergence properties of the various methods for $\zeta^{(2)}$. Figure 1a and Figure 1b show the rate of convergence of each method as the method converges to itself. Figure 2a and Figure 2b show the error (compared to the exact solution) of the method versus the iteration number. Lastly, Figure 3a and Figure 3b detail the error of each method as the number of grid points N_x is varied. As the domain in question is periodic, the implementation of these methods makes use of the efficient fast Fourier transform, and as such the values chosen for N_x were restricted to 8, 16, 32, 64 and 96. While 8, 16, 32 and 64 would be typical choices to use with the fast Fourier transform, 96 (not 128) is the next and last value tested as a means of displaying one common aspect of inverse problems. As the number of gridpoints increases, the accuracy increases but the stability decreases (5). This means that there is some optimum choice for N_x. The error generally decreases as N_x is increased to 64, but several methods fail to converge at $N_x = 128$, therefore, $N_X = 96$ was the last value tested.

5.3 Representative Results

The next figures Figure 4 and Figure 5, will graphically compare the outputs of the methods (including Craig's formula) for $\zeta^{(1)}$ and $\zeta^{(2)}$ with the given parameters in Remark 5.1.1. There are a few things of note in these representative results. Not surprisingly, the methods of the same order perform comparably. In Figure 4a and Figure 5a, it is easy to distinguish Craig's formula from the second and fifth order algorithms, however the second order methods are not

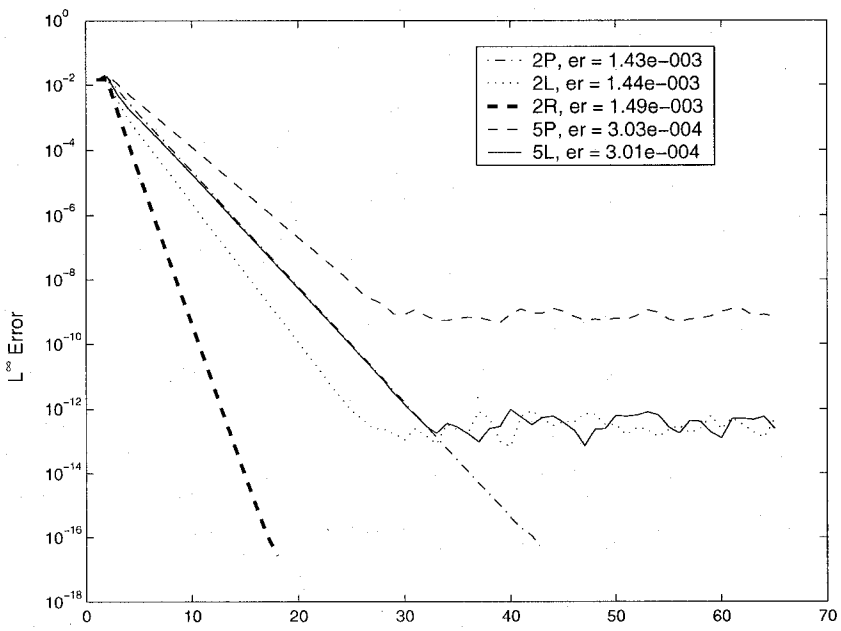

Figure 1a. Convergence of Methods for $\zeta^{(1)}$

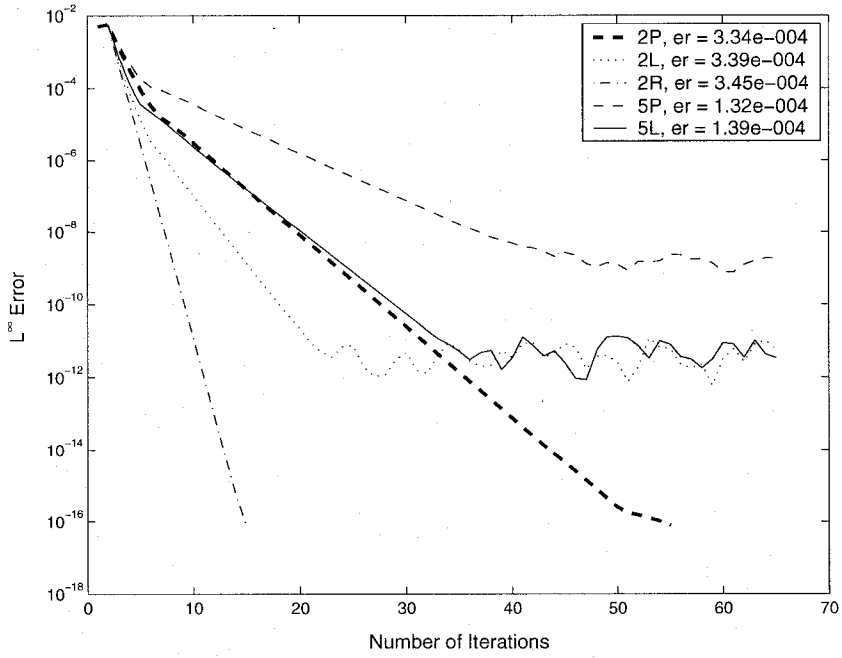

Figure 1b. Convergence of Methods for $\zeta^{(2)}$

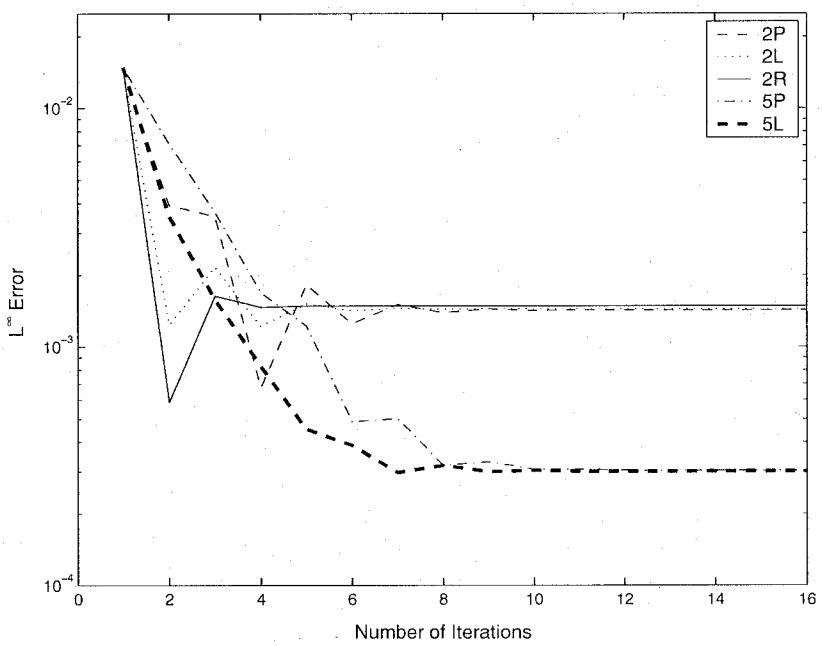

Figure 2a. Convergence Towards Input for $\zeta^{(1)}$

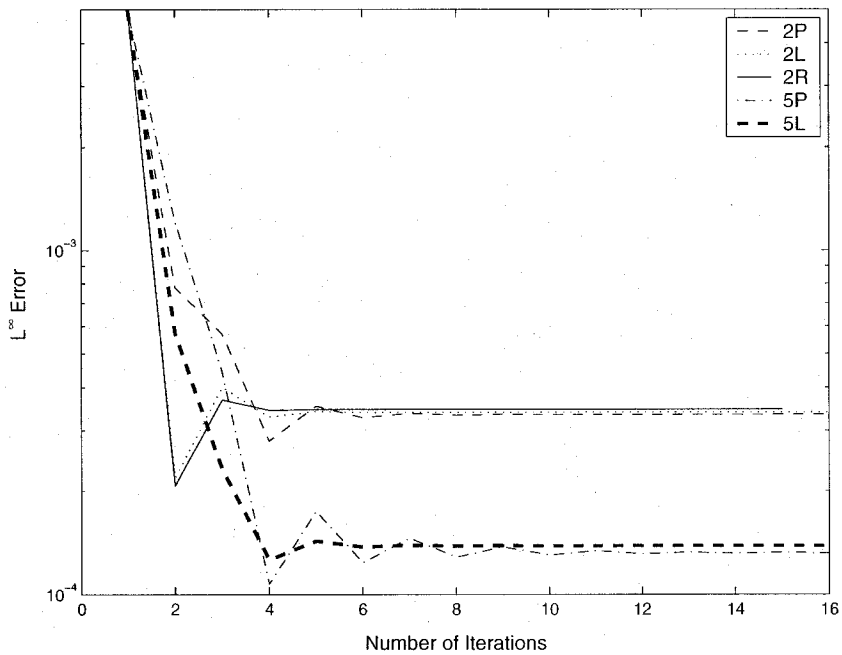

Figure 2b. Convergence Towards Input for $\zeta^{(2)}$

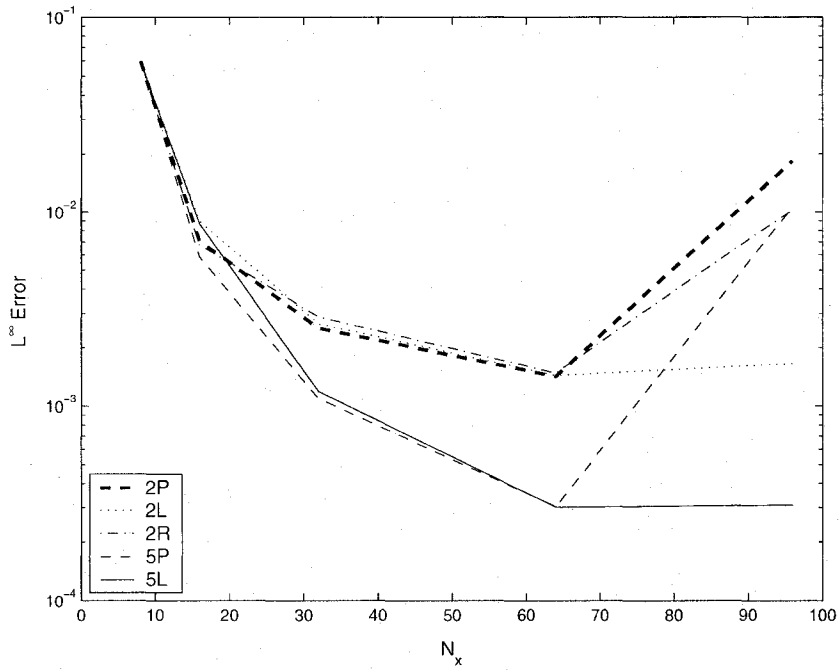

Figure 3a. Error vs. Number of Gridpoints for $\zeta^{(1)}$

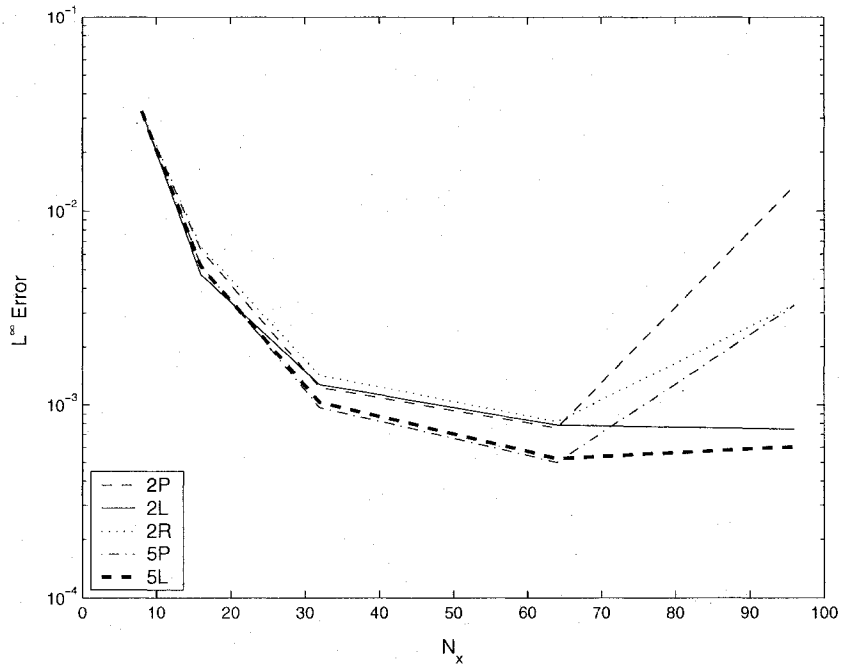

Figure 3b. Error vs. Number of Gridpoints for $\zeta^{(2)}$

easily distinguishable from the fifth order methods. The differences between all of the methods are most profound at the crest of the deformation. Therefore, to see the difference between the second and fifth order methods, in Figure 4b and Figure 5b we zoom in around the crests to show the differences between the second order and fifth order methods.

For both bottom profiles, the first order approximation (Craig's formula) reasonably reconstructs the general shape of the input data, but over-exaggerates the amplitude of the bottom deformation. The second order approximations improve on the accuracy of the magnitude of the amplitude, and the fifth order methods improve the accuracy even more. Both of these examples are meant to be representative as to how well the algorithms can work, and while the set parameters are all of moderate value, they by no means represent the smallest error that the algorithms produce for the families of functions ζ_1 and ζ_2.

5.4 Variation of Parameters in $\zeta_1(x)$

The various bottom topographies defined by the family of functions $\zeta^{(1)}$ have three parameters; a defines the amplitude of the Gaussian bump, b defines the slope of the sides of the bump, and h is the reference depth. The following figures will show how well the various methods perform while these parameters are varied. While each individual parameter is varied the others will be held constant at their previous values (see Remark 5.1.1). Figure 6a, Figure 6b and Figure 6c profile the errors of the various methods while varying the parameters a, b and h respectively.

We notice in Figure 6a that the errors of all the methods while varying a increase nearly linearly (on the log plot) and then shoot upward and vary wildly when the value of a becomes

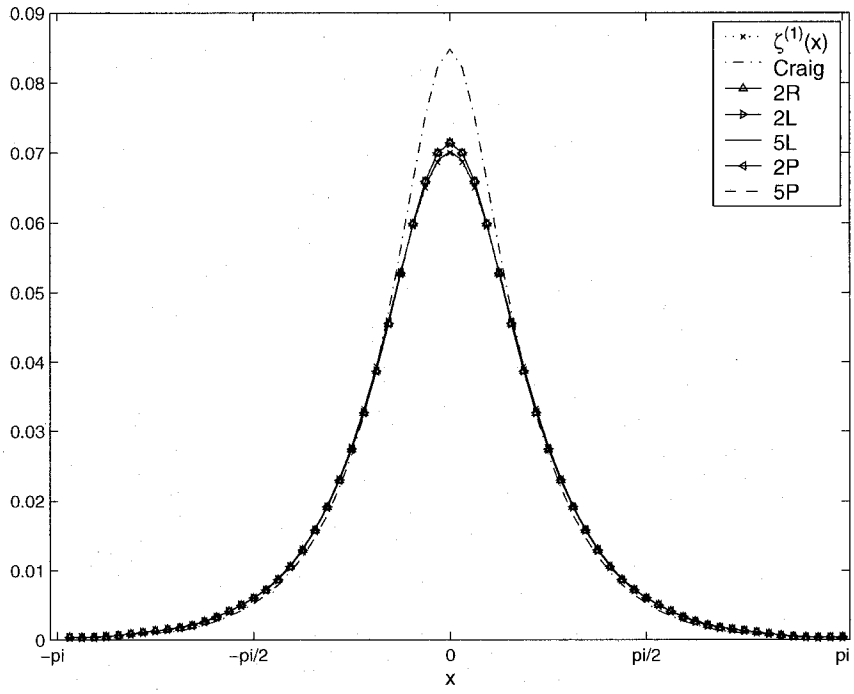

Figure 4a. Representative Results For $\zeta^{(1)}$

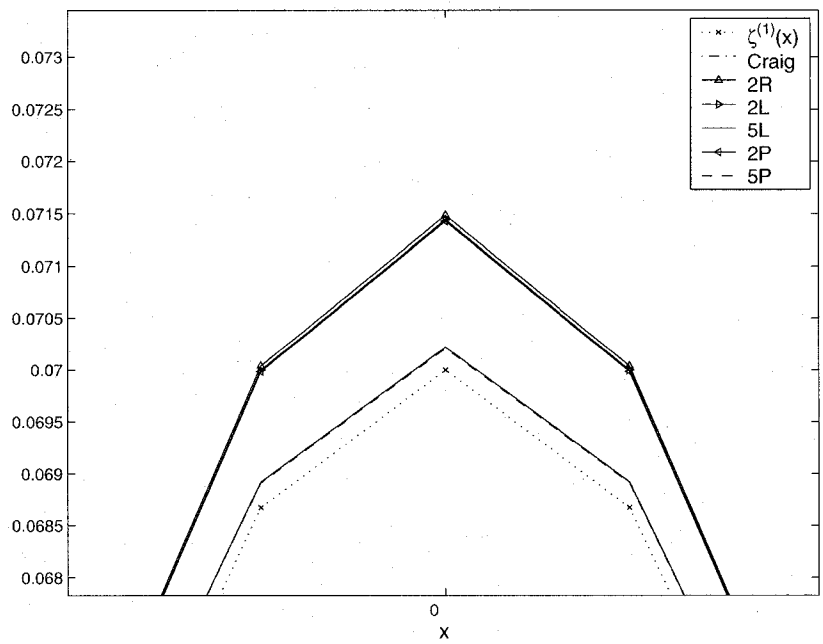

Figure 4b. Representative Results For $\zeta^{(2)}$

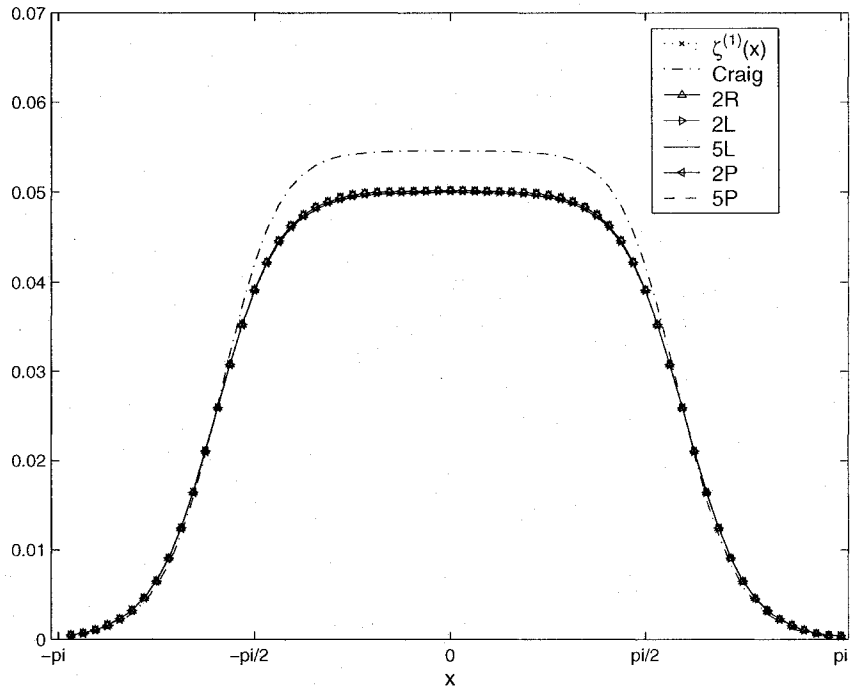

Figure 5a. Magnified Representative Results For $\zeta^{(1)}$

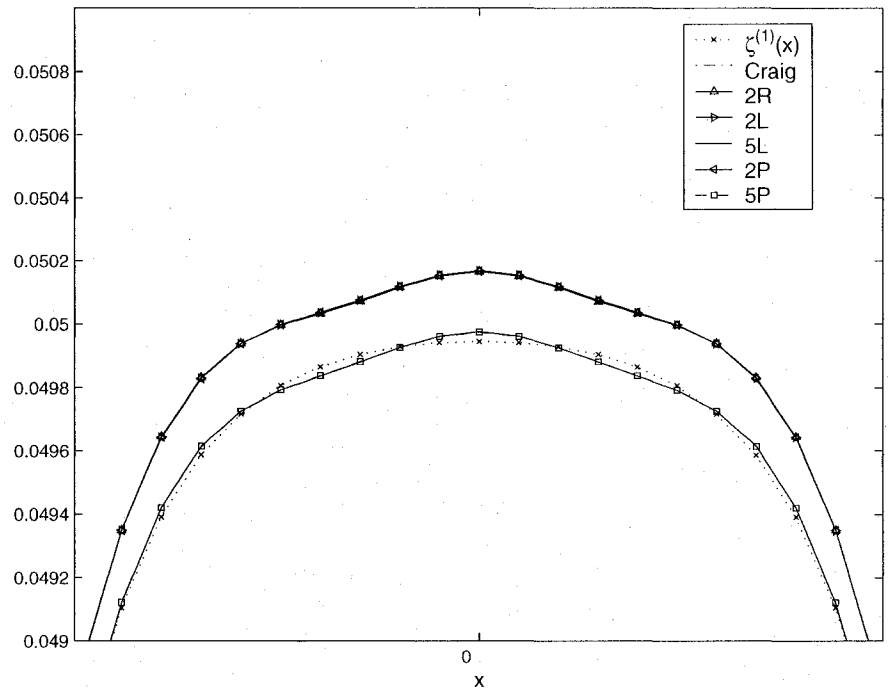

Figure 5b. Magnified Representative Results For $\zeta^{(2)}$

too great for the individual methods, with the lone exception of 2R. At this point it might be interesting to note that 2R, while not as accurate as the fifth order methods, converges quite a bit faster than any of the other second order or higher methods, and it seems to have a wider range of applicability. Again, in what will become a recurring theme, different methods of the same order, perform virtually identically within their respective range of applicability. Picard iteration, however, typically has a smaller range of applicability than the factored methods, and while 2R has a much larger range of applicability.

Figure 6b shows a very interesting characteristic in the fifth order methods for the parameter b. It appears that there is some sort of "best case steepness" in which the fifth order methods perform almost an entire order of magnitude better than the second order methods. Outside of this range ($b > 5$), all of the higher order methods are comparable in accuracy.

In Figure 6c, it can be seen that when h is varied, again the same order methods perform comparably. For each method there is some maximum depth h where the method can no longer be applied. This is the only apparent difference between methods of comparable order. The left factored methods outperform the equivalent methods of similar order. It is interesting to note that the Picard iterations have the same blow up value for h, and the 2R slightly outperforms the second order Picard method.

5.5 Variation of Parameters in $\zeta_2(x)$

In Figure 7a-Figure 7d the parameters $a, b, c,$ and h in the family of functions ζ_2 are varried. For a, b and h, the plot of the errors are, not surprisingly, quantitatively similar to the corresponding graphs for $\zeta^{(1)}$. One major difference between varying a in $\zeta^{(2)}$ as opposed to

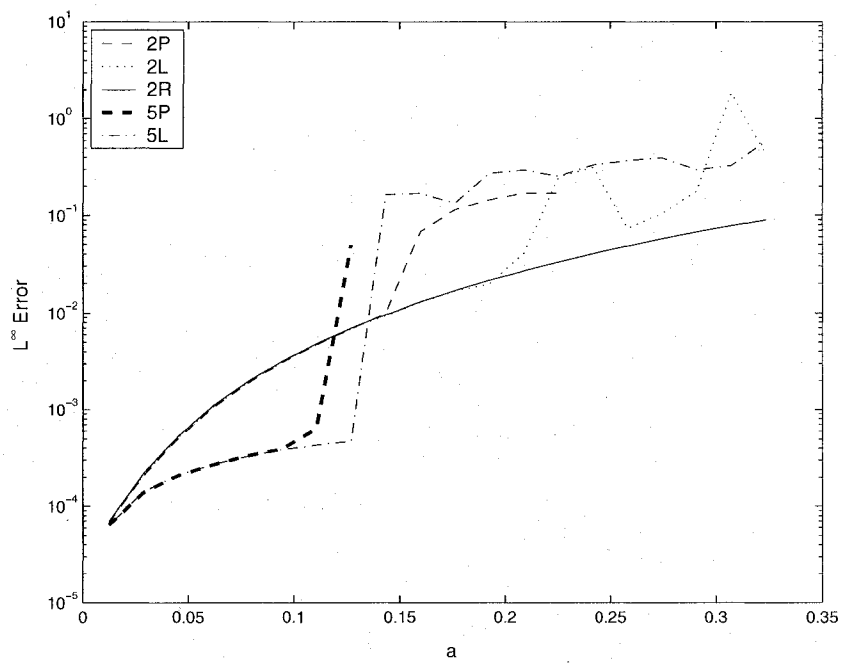

Figure 6a. Error vs. a for $\zeta^{(1)}$

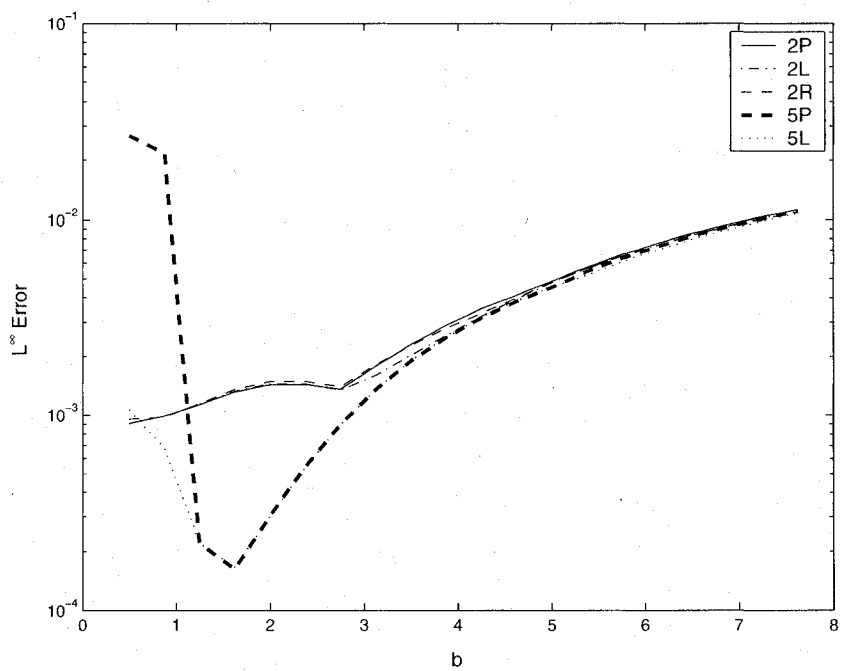

Figure 6b. Error vs. b for $\zeta^{(1)}$

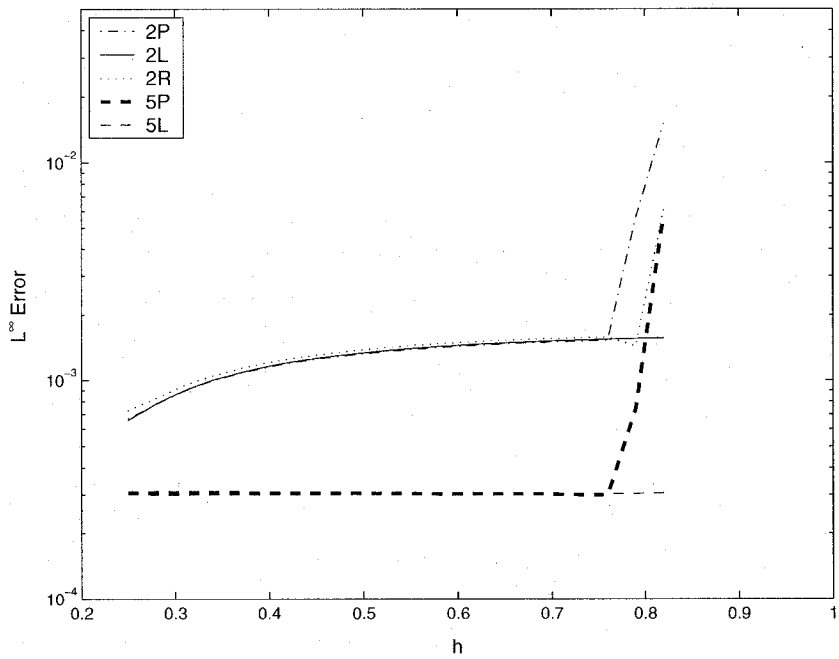

Figure 6c. Error vs. h for $\zeta^{(1)}$

$\zeta^{(1)}$ should be pointed out. Since $\zeta^{(2)}$ adds two hyperbolic tangent functions together, it will have an amplitude of almost twice the value of a specified. For example, if a is given the value .025 for $\zeta(2)$, $\zeta^{(2)}$ will have an amplitude of .05.

One observation of note for the parameter a is that the range where the fifth order methods outperform the second order methods is much smaller than the range of a for $\zeta^{(1)}$, even when the fact that a given value of a for $\zeta^{(1)}$ is twice that of the corresponding value for a in $\zeta^{(2)}$. Also, the method 5P simply fails to converge when a is larger than the quite moderate value

of .03. The 5L method losses its superiority over the second order methods at the same value of a where 5P fails, but it still does converge to something. Continuing a theme seen in earlier pictures, the 2R method outperforms the other second order methods by far in terms of range of applicability. Along these lines, 2L also outperforms 2P.

Figure 7b yields nearly identical properties to Figure 6b as far as how the different methods compare when b is varied. One interesting point is that as $b \to \infty$, the sandbar is transformed into a flat "table top" type figure. If Figure 7b was extended further, it would appear that the errors do level out. This implies that the various methods might be able to reasonably reconstruct bottom contours that have points and edges to them. The case of a flat table top will be an example used in a later section that will showcase some representative results for other curious examples of bottom contours.

Figure 7c shows some very peculiar results. Not surprisingly, the comparable order methods all perform similarly, and perform fairly well. There is not, however, the nice smooth, gradual changes in error as seen when other parameters are varied. As c is increased past a certain value (approximately 2), the function $\zeta^{(2)}$ forms a corner at $x = \pm\pi$, so it is not surprising that as c increases the error does go up.

When h is varied, the only qualitative difference between Figure 7d and Figure 6c is that, for a very small neighborhood, the second order algorithms actually outperform the fifth order algorithms. While the error for the second order algorithms are fairly constant in Figure 6c, in Figure 7d the error decreases at first as h increases, and then gradually increases until h is too large and the methods become unreliable.

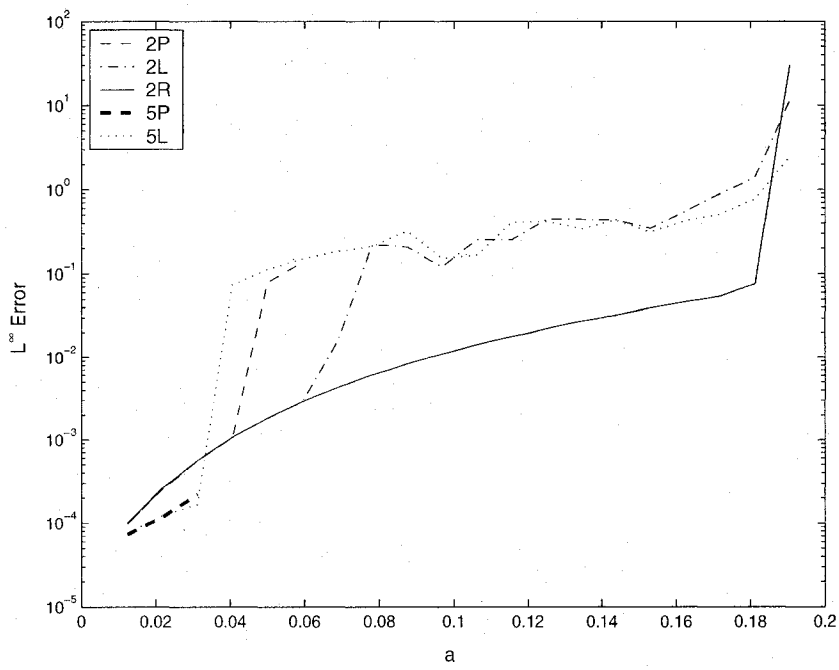

Figure 7a. Error vs. a for $\zeta^{(2)}$

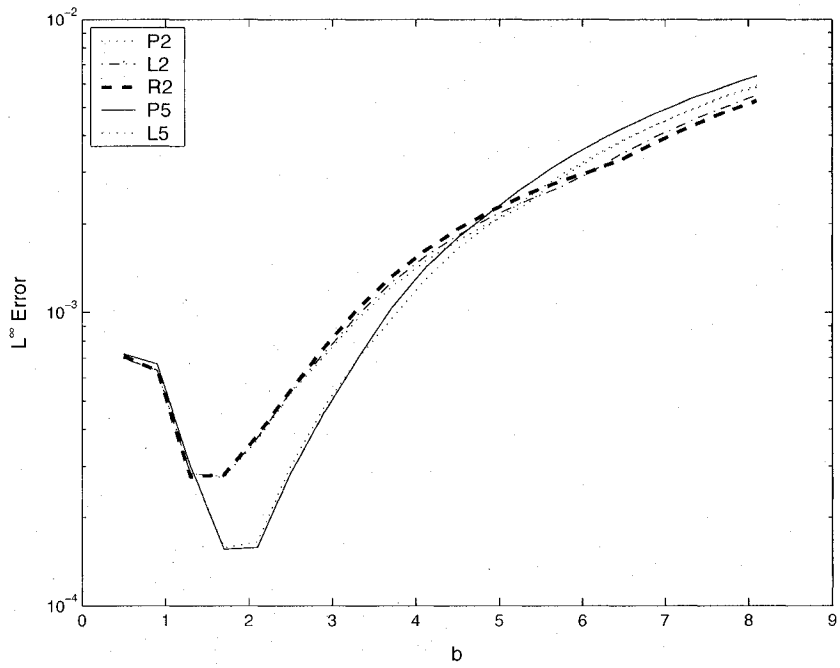

Figure 7b. Error vs. b for $\zeta^{(2)}$

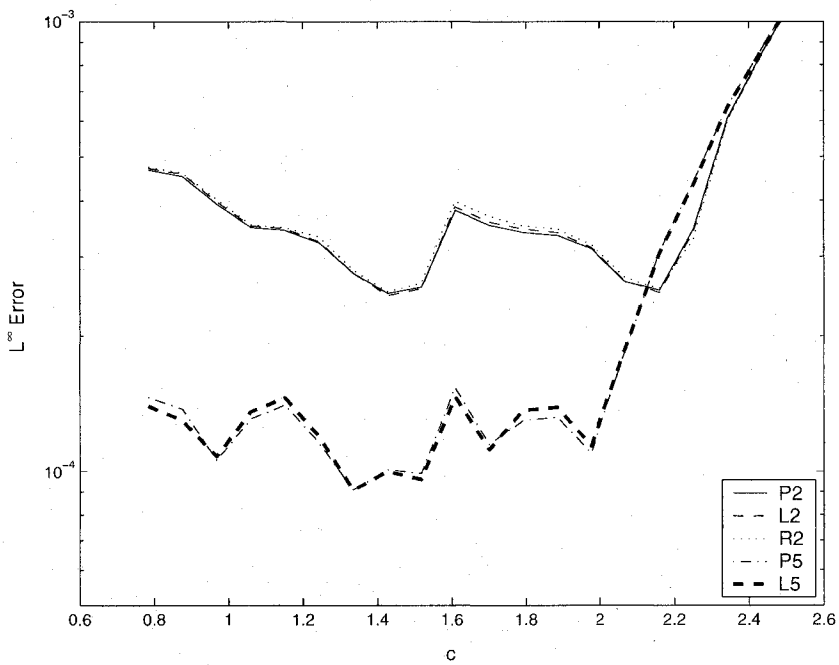

Figure 7c. Error vs. c for $\zeta^{(2)}$

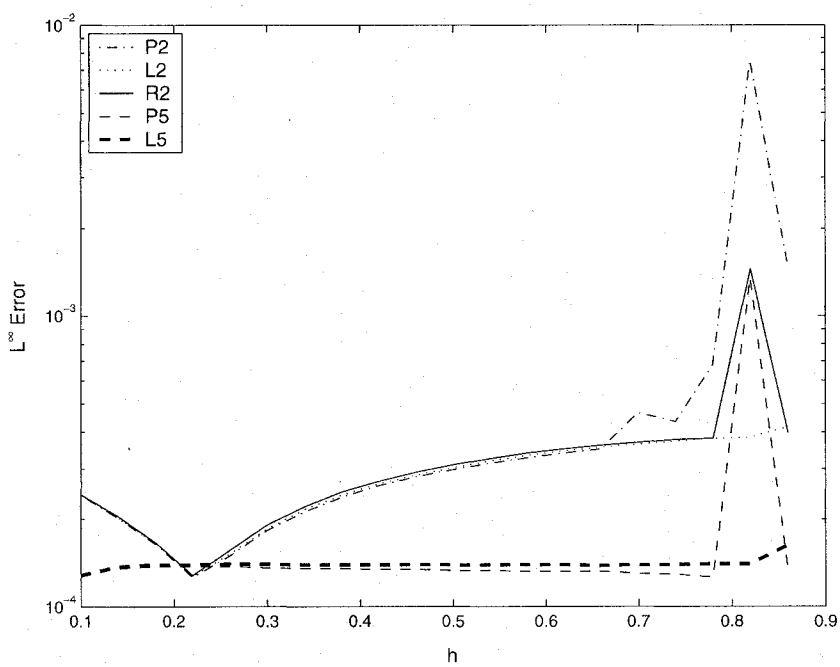

Figure 7d. Error vs. h for $\zeta^{(2)}$

5.6 Noise

Noise will first be added to $\overline{\eta}$, and then it will be added to ω. The noise will be uniform, and generated in the following manner. A random number generator is used to generate a vector the length of $\overline{\eta}$ (in the case of adding noise to ω, the noise will be a scalar) with values ranging from zero to one. That vector (scalar) is then scaled so that the values of the noise vector fell between $1 - p$ and $1 + p$, where $p = \{.0001, .001, .01, .1\}$. The first two figures, Figure 8a and Figure 8b detail the error as the noise applied to $\zeta^{(1)}$ and $\zeta^{(2)}$ is increased from .01% to 10%. The next two figures, Figure 9a and Figure 9b, detail the error as noise is applied to the frequency ω, in a similar manner as it was added to $\overline{\eta}$ (but now the noise is just a scalar).

5.7 Representative Results–Miscellaneous Bottom Contours

The following few figures are some extra curious examples in attempts to see how far these methods can stretch. Included in these (Figure 10a), is the limiting case of the $\zeta^{(2)}$ family when $c \to \infty$. Also highlighted is the case of ζ with a sharp crest (Figure 10b), and an antisymmetrical example (Figure 10c).

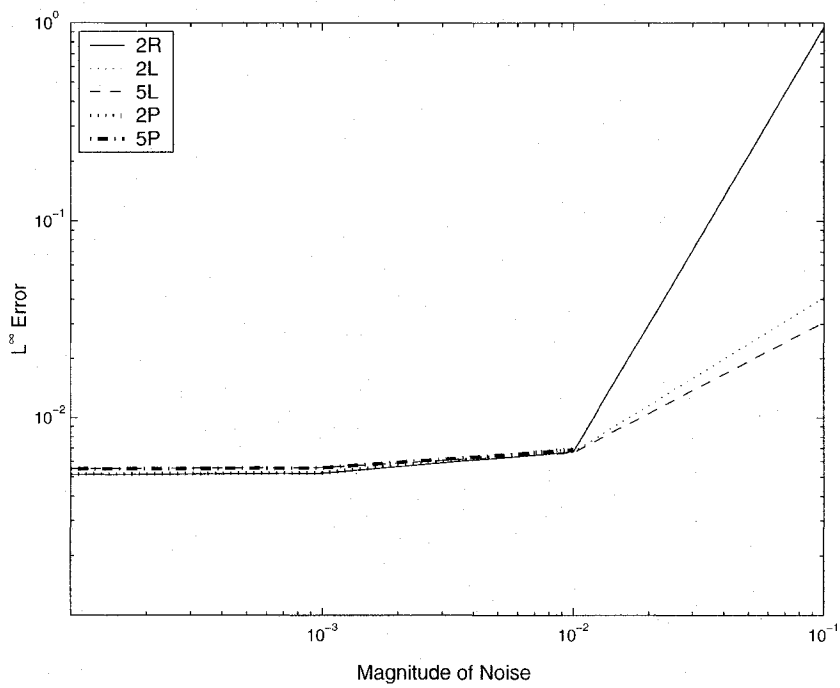

Figure 8a. Error vs. Noise Magnitude in $\overline{\eta}$ for $\zeta^{(1)}$

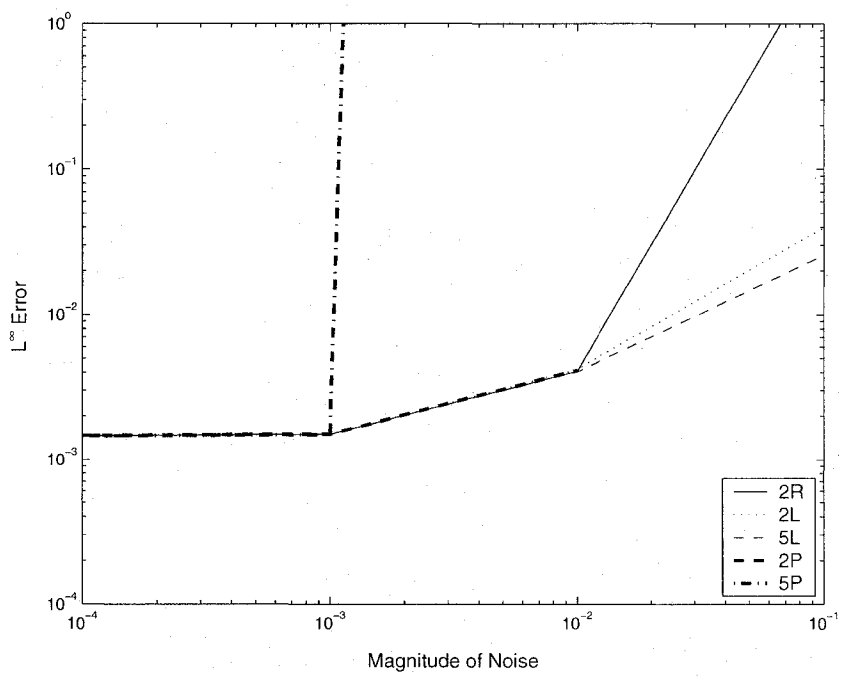

Figure 8b. Error vs. Noise Magnitude in $\overline{\eta}$ for $\zeta^{(2)}$

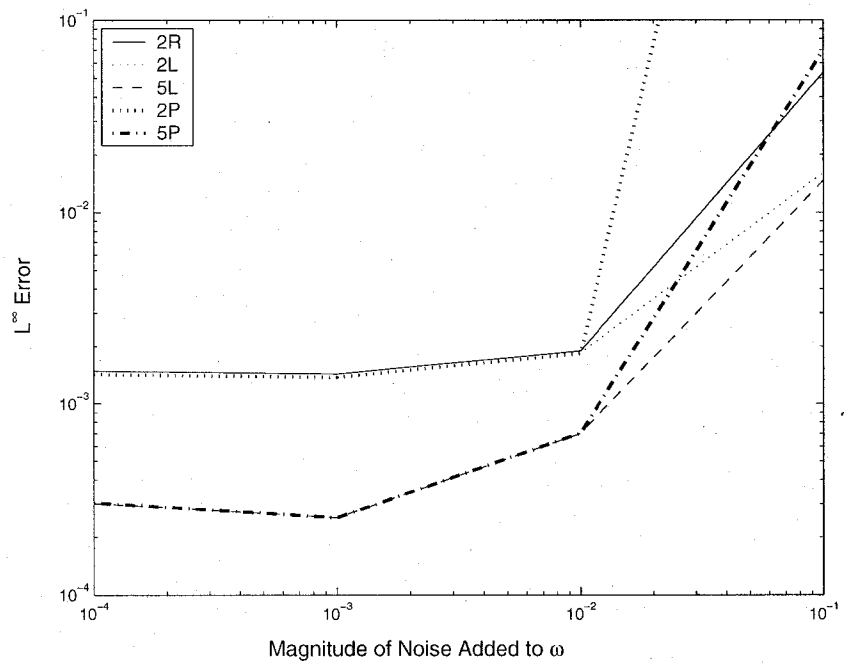

Figure 9a. Error vs. Noise Magnitude in ω for $\zeta^{(1)}$

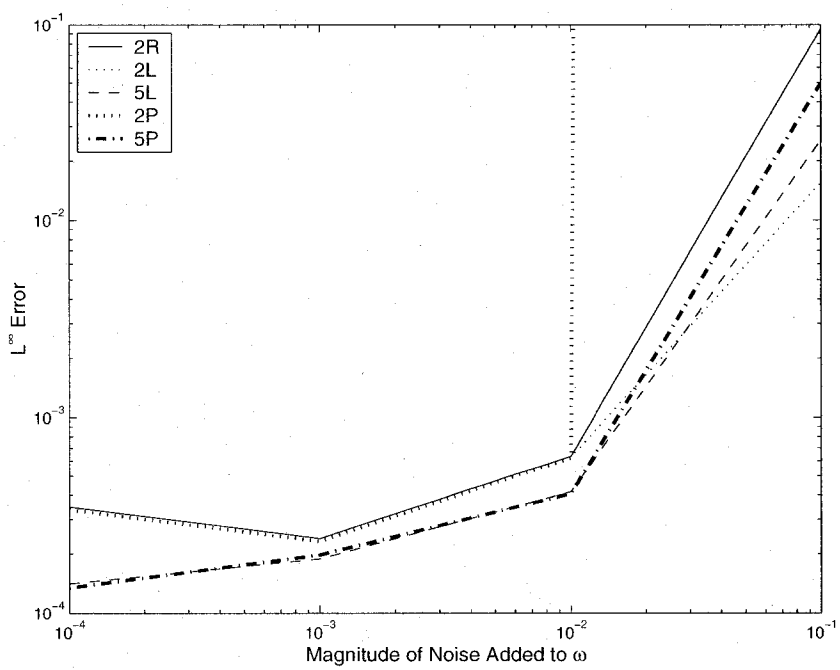

Figure 9b. Error vs. Noise Magnitude in ω for $\zeta^{(2)}$

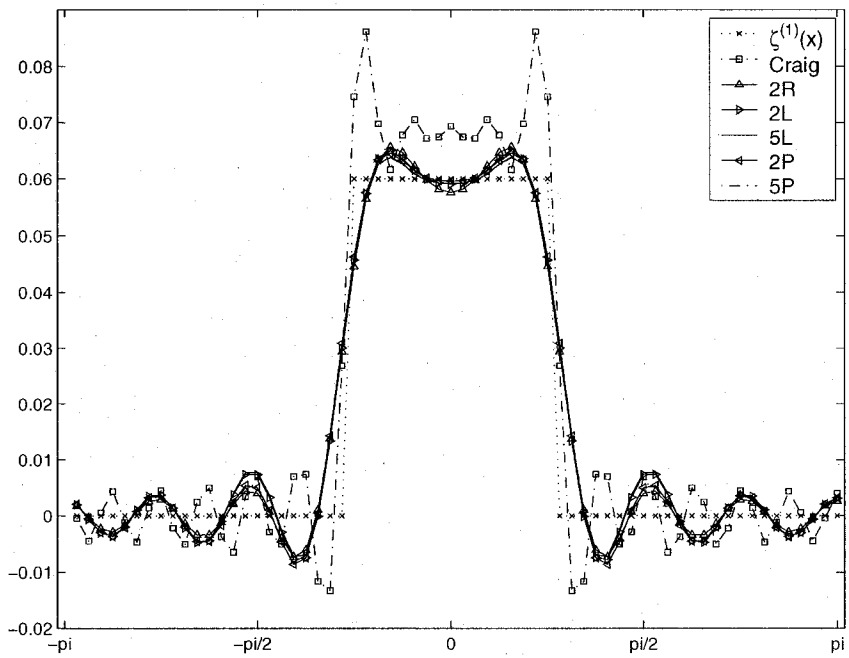

Figure 10a. Limiting Case When $c \to \infty$

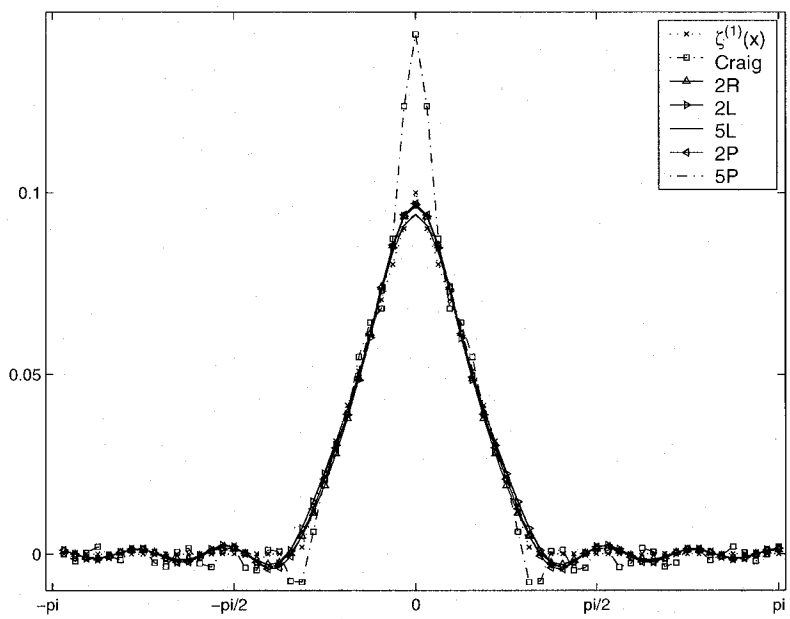

Figure 10b. Representative Results When ζ Has a Sharp Corner

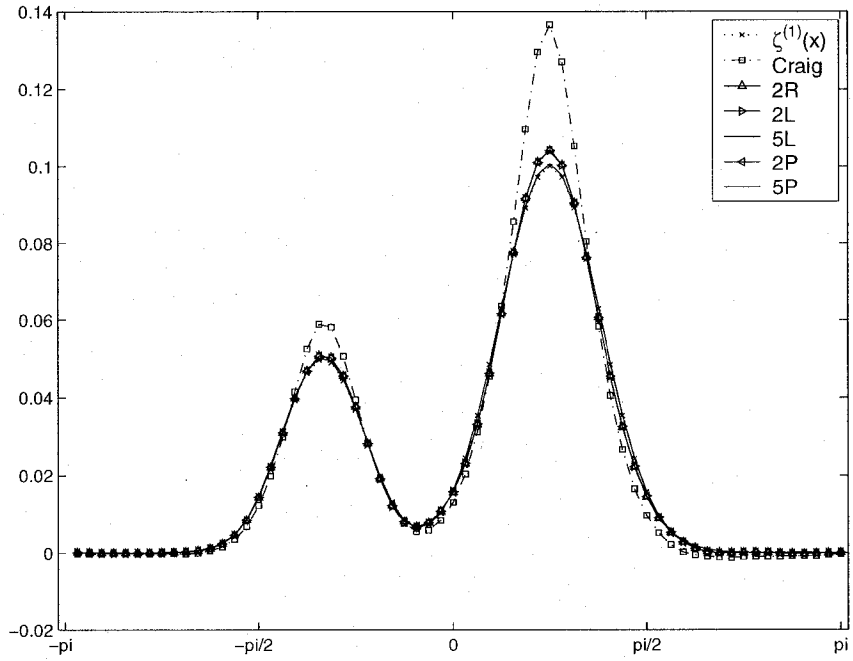

Figure 10c. Representative Results When ζ is Not Symmetrical

CHAPTER 6

CONCLUSIONS

6.1 The Expansion of the DNO

The analyticity of the DNO is a necessary property to justify the expansion of the DNO into a double perturbation series. This series allows a straightforward and stable recursive method for calculating the DNO. While the Operator Expansions and Field Expansions methods might be straightforward and easy to implement, the Transformed Field Expansions yield a straightforward, if a bit involved, method for explicitly calculating the DNO that allows for an inductive estimation of the terms of the expansion, leading to the analyticity result.

The explicit nature of the expansions makes possible the inverse methods proposed in this thesis. Although Operator Expansions and not Transformed Field Expansions were used in the solution to the inverse problem, since so few terms of the expansion were used, the expansion has not reached the point where OE or FE methods might diverge. The OE methods form the basis of simple methods for the inverse problem of detecting ocean bathymetry from surface measurements, which is easy to implement through a Fourier collocation method, extremely fast in execution and superior to Craig's method in terms of accuracy.

6.2 Comparison of Various Methods

While the result that higher order methods are more accurate is not shocking, it is interesting to note that the higher order methods converge slower than lower order methods. While the higher order methods can achieve a higher order of accuracy than lower order methods, their

range of applicability is typically more limited than methods of lower order. Given the relatively high degree of accuracy, faster rate of convergence, and wider range of applicability of lower order methods (especially that of the second order) right factored method, they might often prove more beneficial in practice than higher order methods.

While straightforward and obvious, Picard iteration proves to be an inferior method. It's rate of convergence is slower, its range of applicability is smaller, and as it generalizes to higher order methods breaks down quickly compared to other methods of comparable order. The left factored method shows great promise, especially when use of a higher order method is desirable, as it is vastly superior to a higher order Picard method, both in range and in convergence. It also will allow for more collocation points and a larger reference depth than any of the other methods before the methods become unstable. While the second order, right factored method does not generalize to higher order methods, it is vastly superior in terms of rate of convergence, and is stable for larger magnitudes of deformations than any other method–arguably the most important parameter to be detected.

6.3 Future Directions

One obvious drawback to the general inverse method proposed is the requirement for standing waves. The relaxing of this requirement is necessary for the eventual application of this method to near shore environments. Before this is done, however, these methods need to be tested in three dimensions. Once these issues have been resolved, verifiable laboratory tests should be done on the methods that are developed.

APPENDICES

Appendix A

SOME NOTES ON SINGULAR-VALUE DECOMPOSITION

This appendix is intended to give some background theory of the methods used in approximating $b(x)$ in the equations of the form $b(x)l(x) = r(x)$ seen in Chapter 4. This is a much abridged version of Chapter 4 in (5). For a more detailed discussion, see Chapter 4 of (5) or Chapter 15 of (17). First a few definitions.

Definition A.0.1. *Let X be a Hilbert Space and let $A : X \to Y$ be a compact linear operator, and let $A^* : Y \to X$ be its adjoint (which is then also compact). The nonnegative square roots of the eigenvalues of the nonnegative self adjoint operator $A^*A : X \to X$ are called the* **singular values** *of A.*

Theorem A.0.1. *Let (μ_n) denote the sequence of nonzero singular values of the compact linear operator A (with $A \neq 0$) ordered such that*

$$\mu_1 \geq \mu_2 \geq \mu_3 \geq \cdots$$

and repeated according to their multiplicity. Then there exist orthonormal sequences (φ_n) in X and (g_n) in Y such that

$$A\varphi_n = \mu_n g_n, \qquad A^* g_n = \mu_n \varphi_n, \tag{A.1}$$

for all $n \in \mathbb{N}$. For each $\varphi \in X$ we have the **singular value decomposition**

Appendix A (Continued)

$$\varphi = \sum_{n=1}^{\infty}(\varphi, \varphi_n)\varphi_n + Q\varphi \tag{A.2}$$

with the orthogonal projection operator $Q : X \to N(A)$ *and*

$$A\varphi = \sum_{n=1}^{\infty}\mu_n(\varphi, \varphi_n)g_n. \tag{A.3}$$

Definition A.0.2. *Each system* (μ_n, φ_n, g_n), $n \in \mathbb{N}$, *defined in the theorem above is called a* **singular system** *of* A.

Theorem A.0.2. ***(Picard)*** *Let* $A : x \to Y$ *be a compact linear operator with singular system* (μ_n, φ_n, g_n). *Then*

$$A\varphi = f$$

is solvable for if and only if f *belongs to the orthogonal complement* $N(A^*)^{\perp}$ *and satisfies*

$$\sum_{n=1}^{\infty}\frac{1}{\mu_n^2}|(f, g_n)|^2 < \infty. \tag{A.4}$$

In this case the solution to $A\varphi = f$ *is given by*

$$\varphi = \sum_{n=1}^{\infty}\frac{1}{\mu_n}(f, g_n)\varphi_n. \tag{A.5}$$

The restrictions on f, specifically that the series $\sum_{n=1}^{\infty}\frac{1}{\mu_n^2}|(f, g_n)|^2$ is bounded , often prevent a direct application of Picard's Theorem (which would theoretically give us an exact solution of φ). When the series is on the left hand side of Equation A.5 is unbounded, it would seem that by truncating the infinite sum, that an approximation to φ can be made. This concept leads to the regularization scheme called spectral cut-off. The reason for this being that μ_n approaches

Appendix A (Continued)

0 as $n \to \infty$, making the expression Equation A.5 blow up as $n \to \infty$. Before this concept is stated as a theorem, one last definition needs to be made.

Definition A.0.3. *Let X and Y be normed spaces and let $A : X \to Y$ be an injective bounded linear operator. Then a family of bounded linear operators $R_\alpha : Y \to X$, $\alpha > 0$, with the property of pointwise convergence*

$$\lim_{\alpha \to 0} R_\alpha A\varphi = \varphi \tag{A.6}$$

for all $\varphi \in X$ is called a **regularization scheme** *for the operator A. The parameter α is called the* **regularization parameter**.

With that definition, a spectral cut-off scheme can be rigorously stated.

Theorem A.0.3. *Let A be an injective compact linear operator with singular system (μ_n, φ_n, g_n), $n \in \mathbb{N}$. Then the* **spectral cut-off**

$$R_m f = \sum_{n=1}^{m} \frac{1}{\mu_n}(f, g_n)\varphi_n \tag{A.7}$$

is a regularization scheme with regularization parameter $m \to \infty$ and $\|R_m\| = 1/u_m$.

CITED LITERATURE

1. D. J. Acheson. *Elementary fluid dynamics.* The Clarendon Press Oxford University Press, New York, 1990.

2. Robert A. Adams. *Sobolev spaces.* Academic Press [A subsidiary of Harcourt Brace Jovanovich, Publishers], New York-London, 1975. Pure and Applied Mathematics, Vol. 65.

3. R. Coifman and Y. Meyer. Nonlinear harmonic analysis and analytic dependence. In *Pseudodifferential operators and applications (Notre Dame, Ind., 1984)*, pages 71–78. Amer. Math. Soc., 1985.

4. Michael Collins and W. Kuperman. Inverse problems in ocean acoustics. *Inverse Problems*, 10(5):1023–1040, 1994.

5. David Colton and Rainer Kress. *Inverse acoustic and electromagnetic scattering theory.* Springer-Verlag, Berlin, second edition, 1998.

6. Walter Craig. Personal Communication, 1998.

7. Walter Craig, Philippe Guyenne, David P. Nicholls, and Catherine Sulem. Hamiltonian long wave expansions for water waves over a rough bottom. *Proc. Roy. Soc. Lond., A*, 461(2055):839–873, 2005.

8. Walter Craig and David P. Nicholls. Traveling two and three dimensional capillary gravity water waves. *SIAM J. Math. Anal.*, 32(2):323–359, 2000.

9. Walter Craig, Ulrich Schanz, and Catherine Sulem. The modulation regime of three-dimensional water waves and the Davey-Stewartson system. *Ann. Inst. Henri Poincaré*, 14:615–667, 1997.

10. Walter Craig and Catherine Sulem. Numerical simulation of gravity waves. *Journal of Computational Physics*, 108:73–83, 1993.

11. Lawrence C. Evans. *Partial differential equations.* American Mathematical Society, Providence, RI, 1998.

12. David Gilbarg and Neil S. Trudinger. *Elliptic partial differential equations of second order.* Springer-Verlag, Berlin, second edition, 1983.

13. C. Godrèche, editor. *Solids far from equilibrium.* Cambridge University Press, Cambridge, 1992.

14. Stephan Grilli. Depth inversion in shallow water based on nonlinear properties of shoaling periodic waves. *Coastal Engineering*, 35:185–209, 1998.

15. Philippe Guyenne and David P. Nicholls. Numerical simulation of solitary waves on plane slopes. *Math. Comput. Simul. (to appear)*, 2005.

16. Bei Hu and David P. Nicholls. Analyticity of Dirichlet–Neumann operators on Hölder and Lipschitz domains. *SIAM J. Math. Anal.*, 37(1):302–320, 2005.

17. Rainer Kress. *Linear integral equations.* Springer-Verlag, Berlin, 1989.

18. N. V. Krylov. *Lectures on Elliptic and Parabolic Equations in Hölder Spaces.* American Mathematical Society, Providence, RI, 1997,.

19. Olga A. Ladyzhenskaya and Nina N. Ural'tseva. *Linear and quasilinear elliptic equations.* Academic Press, New York, 1968.

20. Horace Lamb. *Hydrodynamics.* Cambridge University Press, Cambridge, sixth edition, 1993.

21. David P. Nicholls and Fernando Reitich. A new approach to analyticity of Dirichlet-Neumann operators. *Proc. Roy. Soc. Edinburgh Sect. A*, 131(6):1411–1433, 2001.

22. David P. Nicholls and Fernando Reitich. Analytic continuation of Dirichlet-Neumann operators. *Numer. Math.*, 94(1):107–146, 2003.

23. David P. Nicholls and Mark Taber. Joint analyticity and analytic continuation for dirichlet-neumann operators on doubly perturbed domains. *Journal of Mathematical Fluid Mechanics, accepted* 2006.

24. Cynthia Piotrowski and John Dugan. Accuracy of bathymetry and current retrievals from airborne optical time–series imaging of shoaling waves. *IEEE Transactions on Geoscience and Remote Sensing*, 40(12):2606–2618, 2002.

25. Ulrich Schanz. *On the Evolution of Gravity-Capillary Waves in Three Dimensions.* PhD thesis, University of Toronto, 1997.

26. Ralph A. Smith. An operator expansion formalism for nonlinear surface waves over variable depth. *J. Fluid Mech.*, 363:333–347, 1998.

27. Michael Taroudakis and George Makrakis. *Inverse problems in underwater acoustics.* Springer–Verlag, New York, 2001.

28. Vladimir Zakharov. Stability of periodic waves of finite amplitude on the surface of a deep fluid. *Journal of Applied Mechanics and Technical Physics*, 9:190–194, 1968.

VITA

MARK TABER

Office:

Dept. of Mathematics, Stat., and Comp. Sci.

University of Illinois at Chicago (M/C 249)

859 S Morgan St.

Chicago, IL 60611

Phone: (312) 413–8267

FAX: (312) 996–1491

E-Mail: mtaber2@math.uic.edu

Home:

455 E Ohio St. Apt. 1115

Chicago, IL 60611

Phone: (312) 245-9377

RESEARCH INTERESTS

Water waves and fluid dynamics; free boundary problems; inverse problems, numerical methods for the solution of partial differential equations, surface elements.

EDUCATION

Ph. D. Mathematics, University of Illinois at Chicago, Chicago, IL. May 2007.

Sc. M. Mathematics, University of Notre Dame, Notre Dame, IN. May 2004.

B. S. Mathematics, Pacific Union College, Angwin, CA. June 2002.
Magna Cum Laude.

PUBLICATIONS

Mathematical Properties of the Dirichlet-Neumann Operator and its Application to a water wave inspired inverse problem. Ph.D. thesis, University of Illinois at Chicago, *in preparation 2007.*

PUBLICATIONS continued...

(with David P. Nicholls) Joint Analyticity and Analytic Continuation of Dirichlet-Neumann Operators on Doubly Perturbed Domains. *Journal of Mathematical Fluid Mechanics* (accepted 2006).

(with David P. Nicholls) A New Method for Determining Ocean Bathymetry from Surface Wave Measurements. *in preparation.*

INVITED PRESENTATIONS

"5th International IMACS Conference on Nonlinear Evolution Equations and Wave Phenomena: Computation and Theory," Minisymposium-Numerical Methods for Nonlinear Dispersive Wave Equations, University of Georgia, Athens, GA, April 16-19, 2007.

"Mathematics and its Applications Seminar," University of Illinois at Chicago, October 11, 2006.

CONFERENCES & WORKSHOPS

"5th International IMACS Conference on Nonlinear Evolution Equations and Wave PHenomena," University of Georgia, Athens, Georgia, April 16-19, 2007.

"SIAM Annual Meeting," Boston, MA, July 10-July 14, 2006.

"AMS Spring Central Sectional Meeting," University of Notre Dame, Notre Dame, IN April 8-9, 2006.

"4th International IMACS Conference on Nonlinear Evolution Equations and Wave Phenomena," University of Georgia, Athens, Georgia, April 11-14, 2005.

CONFERENCES & WORKSHOPS continued...

"Workshop on Free Surface Waver Waves," Fields Institute, Toronto, Canada, June 14-18, 2004.

"Workshop on Nonlinear Wave Equations," Fields Institute, Toronto, Canada, March 15-19, 2004.

"PDE's and Their Applications," University of Notre Dame, Notre Dame, IN, Aug 2003.

TEACHING EXPERIENCE

Teaching Assistant, Calculus I (Mathematics 180),
University of Illinois at Chicago, Fall 2006.

Instructor, Calculus III (Mathematics 210),
University of Illinois at Chicago, Spring 2006.

Teaching Assistant, Calculus II (Mathematics 181),
University of Illinois at Chicago, Fall 2005.

Instructor, Calculus I (Mathematics 125),
University of Notre Dame, Spring 2005.

Teaching Assistant, Calculus I (Mathematics 125),
University of Notre Dame, Fall 2004, Fall 2003.

Instructor, Probability (Mathematics 323),
University of Notre Dame, Summer 2004.

Teaching Assistant, Calculus II (Mathematics 126) University of Notre Dame, Spring 2004.

Memberships

American Mathematical Society

Society of Industrial and Applied Mathematics

REFERENCES

Professor David P. Nicholls
Dept. of Math., Stat., and Comp. Sci.
Univ. of Illinois at Chicago (M/C 249)
Chicago, IL 60611
(312) 413–1641
nicholls@math.uic.edu

Professor Jerry Bona
Dept. of Math., Stat., and Comp. Sci.
Univ. of Illinois at Chicago (M/C 249)
Chicago, IL 60611
(312) 996–3044
bona@math.uic.edu

Professor Susan Friedlander
Dept. of Math., Stat., and Comp. Sci.
Univ. of Illinois at Chicago (M/C 249)
Chicago, IL 60611
(312) 413–2167
susan@math.uic.edu

Professor A Alexandrou Himonas
Department of Mathematics
274 Hurley Hall
University of Notre Dame
Notre Dame, IN 46556-4618
(574) 631–7583
Alex.A.Himonas.1@nd.edu